RESEARCH ARTICLE

Key Points:
- Benthic foraminiferal clumped isotope and Mg/Ca temperature proxies are compared in the context of middle Miocene climate change
- Results of the two proxies agree well at ODP Site 761, exhibiting relatively warm bottom water temperatures up to 9°C warmer than today
- The warm temperatures lead to reconstruction of relatively heavy seawater $\delta^{18}O$ compared to modern, especially after ~13 Ma

Supporting Information:
- Supporting Information S1

Correspondence to:
S. E. Modestou,
sevasti.modestou@uib.no

Warm Middle Miocene Indian Ocean Bottom Water Temperatures: Comparison of Clumped Isotope and Mg/Ca-Based Estimates

S. E. Modestou[1,2] , T. J. Leutert[1,2] , A. Fernandez[1,2] , C. H. Lear[3] , and A. N. Meckler[1,2]

[1]Department of Earth Sciences, University of Bergen, Bergen, Norway, [2]Bjerknes Centre for Climate Research, Bergen, Norway, [3]School of Earth and Ocean Sciences, Cardiff University, Cardiff, UK

Abstract The middle Miocene is an important analogue for potential future warm climates. However, few independent deep ocean temperature records exist, though these are important for climate model validation and estimates of changes in ice volume. Existing records, all based on the foraminiferal Mg/Ca proxy, suggest that bottom water temperatures were 5–8°C warmer than present. In order to improve confidence in these bottom water temperature reconstructions, we generated a new record using carbonate clumped isotopes (Δ_{47}) and compared our results with Mg/Ca-based estimates for the Indian Ocean at ODP Site 761. Our results indicate temperatures of 11.0 ± 1.7°C during the middle Miocene Climatic Optimum (MCO, 14.7–17 Ma) and 8.1 ± 1.9°C after the middle Miocene Climate Transition (MCT, 13.0–14.7 Ma), values 6 to 9°C warmer than present. Our record also indicates cooling across the MCT of 2.9 ± 2.5°C (uncertainties 95% confidence level). The Mg/Ca record derived from the same samples indicates temperatures well within uncertainty of Δ_{47}. As the two proxies are affected by different non-thermal biases, the good agreement provides confidence in these reconstructed temperatures. Our Δ_{47} temperature record implies a ~0.6‰ seawater $\delta^{18}O$ change over the MCT, in good agreement with previously published values from other sites. Our data furthermore confirm overall high seawater $\delta^{18}O$ values across the middle Miocene, at face value suggesting ice volumes exceeding present-day despite the warm bottom water temperatures. This finding suggests previously underappreciated additional influences on seawater $\delta^{18}O$ and/or a decoupling of ice volume and ocean temperature.

Plain Language Summary In the context of understanding global warming, the middle Miocene (approximately 12 to 18 million years ago) is an important time in Earth's geological history because atmospheric carbon dioxide levels in parts of this time period were comparable to those predicted for the near future. An accurate understanding of the temperature of deep ocean water in the past is an important constraint for climate studies because that information is needed in order to understand important processes such as ocean heat transport and sea level changes. In this study, we compared the only two temperature proxies available for ancient bottom water, the Mg/Ca and carbonate clumped isotope paleothermometers, to help understand their accuracy in estimating temperatures from the middle Miocene period. We found that the two proxies agree well at our study site (Ocean Drilling Program Site 761 in the Eastern Indian Ocean) despite unresolved issues with both proxies, suggesting that the warm temperatures reconstructed are realistic (approximately 11°C between 15 and 17 Ma, and about 8°C between 11.5 and 13 Ma, compared to approximately 2°C today).

1. Introduction

The middle Miocene is a period of strategic importance as a future warm climate analogue: It is the most recent period in geological history with atmospheric CO_2 concentrations relevant to elevated future CO_2 scenarios. The warmer conditions of the middle Miocene Climatic Optimum (MCO; ~17–15 Ma) are associated with CO_2 concentrations ranging from ~400 to 600 ppmv (Badger et al., 2013; Greenop et al., 2014; Ji et al., 2018; Kürschner et al., 2008; Sosdian et al., 2018; You et al., 2009; Zhang et al., 2013) and global temperatures were significantly warmer than present. Higher temperatures are well documented in terrestrial environments (e.g., Pound et al., 2012), including significantly warmer than modern conditions on the Antarctic continent (Feakins et al., 2012; Lewis et al., 2008; Warny et al., 2009).

The warm MCO was followed by the middle Miocene Climate Transition (MCT; ~13–15 Ma). This subsequent global cooling is associated with a drop in CO_2 concentrations (Badger et al., 2013; Greenop et al., 2014; Kürschner et al., 2008; Sosdian et al., 2018; Super et al., 2018; Zhang et al., 2013), major Antarctic ice sheet (AIS) expansion (see Shevenell and Kennett, 2007, and references therein) and a corresponding ~1‰ increase in benthic foraminiferal $\delta^{18}O$ ($\delta^{18}O_b$; Cramer et al., 2009; Mudelsee et al., 2014; Zachos et al., 2008).

Direct geological, faunal, and floral evidence of AIS retreat and expansion during the MCO and MCT, respectively, comes from the ANDRILL project and Ocean Drilling Program Sites 1165 and U1356 (e.g., Fielding et al., 2011; Hauptvogel & Passchier, 2012; Levy et al., 2016; Passchier et al., 2011; Pierce et al., 2017; Sangiorgi et al., 2018; Warny et al., 2009). This evidence, including sedimentological evidence of significant changes in ice extent, suggests globally observed changes in $\delta^{18}O_b$ over the middle Miocene (Cramer et al., 2009; Mudelsee et al., 2014) were in large part driven by ice volume. It is unclear whether the changes in CO_2 were a driver or consequence (or both) of cooling and increased glaciation. Langebroek et al. (2009) found that there is likely a CO_2 threshold that must be met for initiation of AIS expansion during the middle Miocene. The geological evidence recovered at the ANDRILL sites has also led to the intriguing suggestion that Antarctic ice volume could have been larger than today at times during the middle Miocene (Passchier et al., 2011), a result with significant implications for our understanding of ice sheet behavior.

Ideally, independent temperature estimates are combined with $\delta^{18}O_b$ records to deconvolve the contribution of temperature from the $\delta^{18}O$ of deep ocean water ($\delta^{18}O_{sw}$), in order to estimate changes in global ice volume. For time periods as old as the middle Miocene, there are currently only two proxies independent of $\delta^{18}O$ which can be used to estimate deep sea temperatures: the Mg/Ca and carbonate clumped isotope (Δ_{47}) paleothermometers. To date, only Mg/Ca-based bottom water temperatures have been published for the middle Miocene. Lear et al. (2000) estimated middle Miocene deep sea temperatures to be ~5 to 6°C warmer than modern, taking into consideration multiple sites. Using the revised Mg/Ca temperature calibration of Lear et al. (2002), Billups and Schrag (2003) found slightly warmer temperatures: about 9°C (MCO) and 8°C (post-MCT) in the Indian Ocean, suggesting bottom waters were about 6 to 7°C warmer than modern, and 7.5°C (MCO) and 6°C (post-MCT) in the Southern Ocean, which is about 5 to 7°C warmer than today. These authors also recalculated the Lear et al. (2000) record and derived an approximately 6°C warmer-than-modern multi-site estimate for the middle Miocene. At the high southern latitude Ocean Drilling Program (ODP) Site 1171 (Tasmanian Gateway), Shevenell et al. (2008) estimated maximum temperatures of 7 to 8°C for the MCO and ~6.5°C after the MCT (compared to 0.5°C at present). Those authors also estimated an overall cooling across the MCT of 2 ± 2°C. More recently, applying an updated Mg/Ca calibration taking changes in seawater Mg/Ca into account, Lear et al. (2015) found temperatures at tropical ODP Site 806 (Ontong Java Plateau, Pacific) on average ~8°C warmer than present during the MCO and ~6°C warmer than present after the MCT. Mg/Ca temperature calibrations have evolved to include more complete information, and the effects of non-thermal factors (e.g., seawater Mg/Ca, carbonate saturation state, diagenesis) are better understood (Hollis et al., 2019), but a complete understanding leading to reliable absolute Mg/Ca temperatures has not yet been achieved. The Δ_{47} paleothermometer requires fewer assumptions in comparison (Breitenbach et al., 2018; Evans, Sagoo, et al., 2018) and thus may be an ideal proxy to assess the accuracy of Mg/Ca bottom water temperatures. Using benthic foraminifera from ODP Site 761, this paper compares new Δ_{47} based temperatures with previously published Mg/Ca records from the same site in order to assess the potential of both proxies for reconstructing middle Miocene bottom water temperatures and changes in seawater $\delta^{18}O$.

Every temperature proxy has benefits and drawbacks (Hollis et al., 2019). Mg/Ca analyses can achieve relatively high precision with relatively small amounts of sample material, enabling generation of high temporal resolution records. However, the Mg/Ca ratio of foraminiferal calcite is dependent on several factors other than temperature: Past seawater Mg/Ca, salinity, carbonate ion saturation state, and pH have all been shown to have an effect on Mg/Ca in foraminifera (e.g., Elderfield et al., 2006; Evans et al., 2016; Evans, Müller, et al., 2018; Gray et al., 2018; Marchitto et al., 2007). Mg/Ca temperatures also require species-specific calibrations (e.g., Evans & Müller, 2012), at least in part due to differing sensitivities to non-thermal factors (e.g., Evans et al., 2016). Fortunately, the majority of cosmopolitan deep-dwelling

benthic foraminifera used for geochemical reconstructions of the middle Miocene are extant today, including all species used in the present study.

Direct evidence for past seawater Mg/Ca is relatively sparse. Changes through the Cenozoic are still debated (Broecker & Yu, 2011; Coggon et al., 2010; Evans, Sagoo, et al., 2018; Horita et al., 2002; Lowenstein et al., 2001), and there are particularly few constraints for the middle Miocene (see, for example, Figure 5 of Lear et al., 2015, and Figure 2 of Evans, Sagoo, et al., 2018). Furthermore, changes in sea level due to changes in ice volume and atmospheric CO_2 concentrations were most likely accompanied by changes in the saturation state of deep waters. Carbonate saturation state affects the biological uptake of Mg into benthic foraminiferal calcite (Elderfield et al., 2006) and may have varied, driven largely by variations in seawater $[CO_3^{2-}]$ (Kender et al., 2014). To counter both issues, Lear et al. (2010, 2015) used a benthic foraminifer (*Oridorsalis umbonatus*) which they determined to be less sensitive than other species to changes in seawater Mg/Ca. *O. umbonatus* is also a shallow infaunal species; infaunal foraminifera may be less susceptible to changes in saturation state in certain settings, since they live primarily within pore waters which may maintain a saturation state closer to equilibrium in carbonate rich sediments (Elderfield et al., 2006).

Preservation is also an important consideration for any foraminifera-based proxy, including Mg/Ca. Post-depositional incorporation of inorganic calcite crystals has been argued to incorporate calcite with higher Mg/Ca than primary foraminiferal calcite, which could bias temperature (Bryan & Marchitto, 2008). Ferromanganese (FeMn) oxyhydroxide coatings may contribute excess Mg and increase apparent Mg/Ca (Nairn et al., 2020), while dissolution may preferentially remove Mg from foraminifer tests and decrease apparent Mg/Ca. Well-established cleaning methods (Barker et al., 2003) aim to minimize the impact of trace metal contamination. Nevertheless, specimens should be examined to avoid those showing signs of dissolution or inorganic overgrowths. Diagenesis in the form of closed-system recrystallization is more complex, but Mg/Ca is generally thought to be relatively robust to early-stage recrystallization (Sexton et al., 2006). Thus, preservation is important, but sample screening will alleviate most diagenesis-related problems. The most serious issues to affect Mg/Ca are therefore those which require independent information, such as changes in seawater chemistry affecting the primary uptake of Mg in foraminifera.

More recently, the carbonate clumped isotope (Δ_{47}) paleothermometer has been applied to foraminifera for paleoclimate reconstructions (e.g., Rodríguez-Sanz et al., 2017; Tripati et al., 2014). This proxy involves measurement of the "clumping" or bonding of the heavy rare isotopes ^{13}C and ^{18}O within the same carbonate ion (Eiler, 2007, 2011). Bonds between the heavy rare isotopes are thermodynamically favored at colder temperatures, with no dependence on the fluid isotopic composition in which carbonates form (Eiler, 2011; Schauble et al., 2006).

The abundance of the ^{13}C–^{18}O isotopologue is very low; thus, measurement of m/z 47 relative to m/z 44 as in the case of carbonate-derived CO_2 is imprecise. Consequently, large analytical uncertainties are typically associated with single replicate analyses, and multiple replicate analyses are commonly performed. Compared to Mg/Ca, the application of Δ_{47} requires considerably larger sample sizes, and therefore when working with foraminifera is much more time consuming.

Similarly to Mg/Ca, preservation is also important for Δ_{47}. Recrystallization, precipitation of inorganic calcite, and adherence of carbonate formed in different parts of the water column (such as surface-dwelling coccoliths onto benthic foraminifera) could bias results. Nevertheless, the effect of recrystallization of primary calcite on Δ_{47} is thought to be mitigated in benthic foraminifera (Leutert et al., 2019; Stolper et al., 2018) since this process often occurs relatively early in their burial history (Edgar et al., 2013; Voigt et al., 2015, 2016) and thus at similar temperatures as the primary calcification temperature. To date, it is unknown whether dissolution might affect Δ_{47}. Thorough cleaning is also required for the Δ_{47} proxy to eliminate other adhered carbonates, and a representative number of samples should be examined for preservation and the effectiveness of the cleaning procedure.

The advantages of Δ_{47} lie in the fact that it is independent of seawater chemistry. Past seawater pH, dissolved inorganic carbon, and carbonate saturation state have been shown to have no discernible effect outside analytical uncertainty in the range of pH expected in average marine environments (Eagle et al., 2013; Hill et al., 2014; Kelson et al., 2017; Tang et al., 2014; Tripati et al., 2015; Watkins & Hunt, 2015). Moreover, no species-specific effects have been found for foraminifera (Evans, Badger, et al., 2018; Grauel et al., 2013;

Meinicke et al., 2020; Peral et al., 2018; Piasecki et al., 2019; Tripati et al., 2010). In fact, nearly all carbonates are within error of the same calibration line (Bernasconi et al., 2018; Bonifacie et al., 2017; Kele et al., 2015; Kelson et al., 2017; Tripati et al., 2010), with very few exceptions (e.g., some corals and speleothems; Affek et al., 2008; Eagle et al., 2013; Saenger et al., 2012). Thus, the Δ_{47} paleothermometer is an ideal proxy to compare with Mg/Ca in order to assess the accuracy of the more established Mg/Ca proxy (Breitenbach et al., 2018). Furthermore, similarly to Mg/Ca, Δ_{47} is independent of the $\delta^{18}O$ of the fluid which the carbonate precipitated from (Eiler, 2011; Schauble et al., 2006), and thus, seawater $\delta^{18}O$ can be estimated using the Δ_{47} and $\delta^{18}O_b$ generated from the same measurements. Finally, analytical advances decreasing sample mass requirements (Hu et al., 2014; Meckler et al., 2014; Müller et al., 2017) have made it possible to perform Δ_{47} analyses on downcore foraminifera samples, although more material is still required compared to Mg/Ca. In this regard, foraminiferal Mg/Ca analyses require much less material per analysis, and the analyses themselves are much higher precision; thus, the Mg/Ca proxy can be used to generate much higher resolution temperature records.

2. Materials and Methods

2.1. Setting

Ocean Drilling Program (ODP) Site 761 is located off northwest Australia on the Wombat Plateau (16°44.23′ S, 115°32.10′E) at 2,179 m water depth (Figure 1). The carbonate-rich sediments of Site 761 have been investigated extensively using the Mg/Ca paleothermometer, making this a suitable location to compare the two proxies while examining the thermal history of the deep Indian Ocean. Wombat Plateau sedimentation is characterized as "mature ocean" pelagic since the early Miocene (Exon et al., 1992; von Rad et al., 1992). Benthic foraminifera at this site appear relatively well preserved (Lear et al., 2010). Paleobathymetric indicators suggest that no significant depth changes have occurred since the middle Miocene (Holbourn et al., 2004).

2.2. Sampling

The samples used for this study are the same as those described in Lear et al. (2010), from the middle Miocene section of ODP Site 761B. This allowed for the most direct comparison possible between Mg/Ca and Δ_{47} temperatures, although we could not use the same species of foraminifera (all *Oridorsalis umbonatus* were previously removed for Mg/Ca analysis). The age model is based on biostratigraphy following Holbourn et al. (2004) with ages updated to GTS 2012 (Hilgen et al., 2012), and additional isotope stratigraphy (supporting information Table S2 of Leutert et al., 2020).

Benthic foraminifera (four or more individual tests) were picked from the 250–355 µm size fraction. Note that not all samples contained enough foraminifera for clumped isotope analysis (minimum sample size requirement for one aliquot ~100 µg). The following epifaunal and shallow infaunal species were used: *Cibicidoides wuellerstorfi*, *Cibicidoides mundulus*, *Globocassidulina subglobosa*, *Osangularia culter*, *Pullenia bulloides*, *Gyroidinoides* spp, and other *Cibicidoides* spp.

After collecting foraminifera from either a single sample or two combined adjacent samples, the specimens were gently cracked between glass plates to open all chambers. With the exception of a few samples where *Cibicidoides* spp. or *Cibicidoides wuellerstorfi* and *Cibicidoides mundulus* were grouped together due to low abundances, aliquots for clumped isotope measurement were monospecific. Cracked specimens were transferred to 0.5 ml polypropylene microcentrifuge vials and irrigated with deionized water (~13 MΩ). Samples were cleaned via repeated ultrasonication cycles: the material was irrigated, vortexed, the majority of liquid removed by pipette, and the sample was ultrasonicated. Methanol (ACS reagent grade, Merck) was used for the second cleaning cycle; samples were then cleaned for at least three more cycles with deionized water and ultrasonication, until the supernatant was no longer cloudy. Samples were dried at 50°C in a standard drying oven.

After preparation, a small amount of material (from widely spaced but randomly selected core samples) was transferred to carbon adhesive covered stubs, ensuring different examples of each species employed were selected. Stubs were Au/Pd coated and imaged with a Zeiss Supra 55VP scanning electron microscope (SEM) to check for cleanliness and preservation.
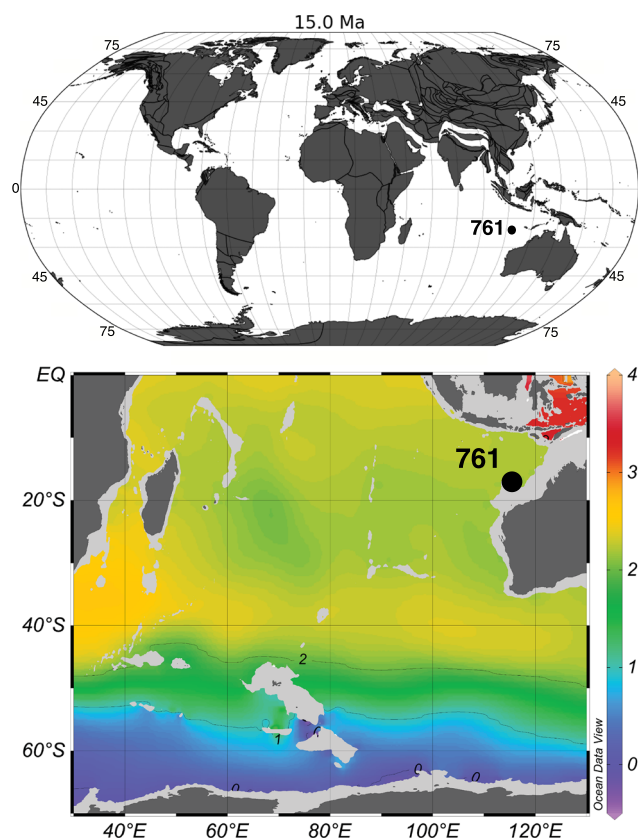
Figure 1. Upper panel, ODP Site 761 location plotted on paleogeography for 15 Ma (map generated using GPlates web portal, http://portal.gplates.org, and plate reconstruction of Matthews et al., 2016). Paleolatitude calculated using paleolatitude.org (Van Hinsbergen et al., 2015). Lower panel, modern water temperatures at 2,200 m water depth (map generated with Ocean Data View, Schlitzer, 2020; data from the World Ocean Database, NOAA).

2.3. Mass Spectrometry

Our analytical approach generally follows previous work (Meckler et al., 2014; Müller et al., 2017). We analyzed Δ_{47} on small carbonate samples using two identical instruments, Thermo Fisher Scientific Kiel IV preparation devices coupled to MAT253Plus gas source isotope ratio mass spectrometers. Individual aliquot mass was 85–105 μg (both machines). The long-integration dual-inlet (LIDI) method (Hu et al., 2014) was employed following Müller et al. (2017). Carbonate digestion was performed using ~104% phosphoric acid at 70°C. CO_2 was purified by diffusion through silver wool and 1.5 cm of PoraPak-Q (ethylvinylbenzene and divinylbenzene copolymer bead) held at −20°C within a sulfinert coated stainless steel tube. Sample gas was passively expanded through a sulfinert coated, stainless steel capillary and measured for 400 s, with signals typically decreasing from 15 to 10 V on m/z 44. Reference gas, starting at matching initial pressure, was measured subsequently from a separate static microvolume. The PoraPak-Q column was heated to 120°C and exposed to high vacuum for at least 1 hr daily for cleaning. The pressure baseline effect (Bernasconi et al., 2013; He et al., 2012) was corrected daily using peak scans, employing a flat region of background as close as possible to the peaks selected from scans at five different intensities (5, 10, 15, 20, and 25 V; Meckler et al., 2014). Sample measurements were corrected following Meckler et al. (2014), with some modifications. We used four carbonate standards of differing $\delta^{13}C$, $\delta^{18}O$, and Δ_{47}; samples and standards were measured in a 1:1 ratio. Three of the standards (ETH1, ETH2, and ETH3) were used to normalize the samples to the absolute reference frame (Dennis et al., 2011), correct for drift in $\delta^{13}C$ and $\delta^{18}O$, and correct scale compression in $\delta^{18}O$. The fourth (ETH4) was used as a consistency standard to monitor instrument performance. The number of replicates of each standard was chosen to improve the accuracy and precision of the empirical transfer function (Kocken et al., 2019). The conversion into the absolute reference frame was performed in a single step using ETH1, ETH2, and ETH3 (without initial offset correction), using

recalculated standard values from Bernasconi et al. (2018). A block of standard measurements, half on either side of any given sample measurement, was used to convert sample data into the absolute reference frame. The number of standards used ranges from 40 to 80, depending on instrument performance during the relevant correction interval. Correction intervals are discrete blocks of time (ranging from weeks to months), demarcated by major maintenance events such as changing reference gas or source tuning. For the correction intervals of this study, the reproducibility of the standards was on average ~0.038‰ (1 SD) for Δ_{47} (reproducibility per correction interval per standard is listed in the supporting information, Tables S1 and S2). Average reproducibility of secondary standard ETH4 was 0.037‰ in Δ_{47}, 0.03‰ in δ^{13}C, and 0.06‰ in δ^{18}O (all 1 SD). All data were processed using the software package Easotope (John & Bowen, 2016) employing IUPAC correction parameters (Brand et al., 2010; Daëron et al., 2016). Further details are published elsewhere (Leutert et al., 2019; Meinicke et al., 2020; Piasecki et al., 2019).

2.4. Δ_{47} Temperature, Seawater δ^{18}O, and Uncertainty Calculations

The small carbonate sample method employed in this study reduces the sample mass needed compared to conventional Δ_{47} measurements. However, many replicate measurements are still required to obtain a reasonably precise estimate of temperature. Based on our current reproducibility and calibration error, a precision of ≤2°C (68% CI) requires samples to be replicated at least 30 times. Consequently, >3 mg of sample are required for a reasonably well-constrained temperature, making it difficult to obtain a temperature value from each individual downcore sample (~30 cm^3 of sediment) when targeting benthic foraminifera. Site 761 was no exception, particularly since we employed samples which had previously been used for Mg/Ca and stable isotope analyses, and thus, the numbers of benthic foraminifera were already somewhat depleted. Although individual samples were replicated more than once where material availability allowed, species-specific replication per sample typically ranged from only one to four measurements (with the exception of two subsamples which generated six and seven species-specific replicates). Furthermore, not all species were abundant enough in every sample to generate any replicate measurements. The solution employed here is to group replicates from different species and adjacent samples together for Δ_{47} (Grauel et al., 2013), acknowledging that this may introduce additional variability. We performed this averaging in two ways: using discrete binning as well as a moving average smoothing function. Discrete sample bins were grouped according to the following criteria, in order of importance: (1) avoiding extended temporal gaps; (2) keeping replicates from the same sample together; and (3) grouping over the shortest interval possible. For this dataset, the maximum bin size possible while maintaining the above criteria is ~30 (measurements); alternatively, smaller bins were tested for comparison. Age ranges, the span between the age of the first and last aliquot within a bin, are indicated by horizontal bars in our figures. We provide confidence intervals (CI) rather than standard error to improve comparability to other records (Fernandez et al., 2017), including the propagated calibration error following Huntington et al. (2009).

The smoothing function employed here is the probabilistic Gaussian window filter (GWF) described in Rodríguez-Sanz et al. (2017), which gives a larger weight to the values nearest the center of the window following a Gaussian probability distribution. We used a 1 Myr window size and a step of 100 kyr. Following those authors, the 5,000 Monte Carlo simulations were performed using a mean equal to the observed Δ_{47} values and an analytical uncertainty equal to the average long-term reproducibility of ETH4. A GWF was then applied to these data, and uncertainties in the final Δ_{47} time series were calculated from the percentiles of the 5,000 simulations. Finally, calibration uncertainty was propagated into the GWF uncertainty again as per Huntington et al. (2009).

Since the relationship between Δ_{47} and temperature is nonlinear, mean Δ_{47} values are determined for each discrete bin or window step prior to calculating temperature. For this study, we employed the Kele et al. (2015) calibration, updated in Bernasconi et al. (2018):

$$\Delta_{47} = 0.0449 \, (\pm 0.001) \cdot 10^6 / T^2 + 0.167 \, (\pm 0.01) \tag{1}$$

Temperatures calculated using this travertine-based calibration are indistinguishable within uncertainty from benthic and planktic foraminifera calibrations performed in our laboratory (Meinicke et al., 2020; Piasecki et al., 2019) though the travertine calibration is based on a wider temperature range. Δ_{47} values are provided with four decimals to avoid rounding errors in subsequent calculations (Tables S1 and S2

and archived raw data, see Acknowledgments). Two replicate analyses, out of a total of 428, were determined to be outliers and removed from the dataset using a 4σ outlier test against the mean of all sample data. No further outlier removal was performed regardless of the method of temperature calculation.

Species-specific $\delta^{18}O$ offsets must be accounted for before calculating $\delta^{18}O_{sw}$, since each temperature is the result of a group of Δ_{47} measurements, and each group includes several species of foraminifera. Offsets were adjusted based on Appendix A of Shackleton et al. (1984), correcting all species to be equivalent to *C. mundulus*. Benthic foraminiferal $\delta^{18}O$ was then averaged for each group, and $\delta^{18}O_{sw}$ was calculated using Equation 9 of Marchitto et al. (2014):

$$\left(\delta^{18}O_b - \delta^{18}O_{sw} + 0.27\right) = -0.245 \cdot BWT + 0.0011 \cdot BWT^2 + 3.58 \tag{2}$$

where BWT is bottom water temperature. Temperatures at 68% and 95% CI were used to estimate $\delta^{18}O_{sw}$ uncertainty in order to focus on the uncertainty derived from the precision of the Δ_{47} temperatures.

2.5. Mg/Ca Temperatures

All *O. umbonatus* Mg/Ca data used to calculate temperatures for Site 761 were originally published in Lear et al. (2010). That work presented two Mg/Ca temperature records by (1) using a linear *Cibicidoides* Mg/Ca-temperature calibration (Marchitto et al., 2007) after subtracting a 0.2 mmol/mol species offset from the *Oridorsalis umbonatus* Mg/Ca data, and (2) temperatures calculated using the same linear temperature sensitivity but with an additional Li/Ca-based carbonate saturation state $(\Delta[CO_3^{2-}])$ correction. Calcium carbonate Li/Ca reflects both seawater saturation state and temperature (Hall & Chan, 2004; Lear & Rosenthal, 2006; Marriott et al., 2004). However, these calibrations do not take into account different seawater Mg/Ca. For this reason, the records derived in Lear et al. (2010) were originally interpreted in terms of relative downcore temperature variations and not absolute temperatures. For that record, the relative temperature variations were considered robust because seawater Mg/Ca (Mg/Ca$_{sw}$) is thought to have changed relatively little over the middle Miocene period investigated (Evans, Sagoo, et al., 2018; Lear et al., 2015). Subsequently, Lear et al. (2015) presented a new calibration describing the sensitivity of *O. umbonatus* to both temperature (via an exponential relationship) and Mg/Ca$_{sw}$ (via a power law relationship) (hereafter L2015):

$$Mg/Ca = A \cdot Mg/Ca_{sw}{}^H \cdot \exp^{(B \cdot BWT)} \tag{3}$$

The constants in the equation (A, H, and B) were determined by examining a suite of samples from the early Eocene, when it can be reasonably assumed there is little to no water storage in ice and therefore the temperature component could be reasonably independently estimated using benthic foraminiferal $\delta^{18}O$ (Lear et al., 2015). Here we recalculated Mg/Ca temperatures for Site 761 using the L2015 calibration as it allows incorporating information about Mg/Ca$_{sw}$ yielding absolute temperature estimates. We used the same values as Lear et al. (2015) for A, B, and H (0.66 ± 0.08, 0.114 ± 0.02 and 0.27 ± 0.06, respectively) and applied a 5-point smoothing to the data consistent with the original publication. A disadvantage of the L2015 calibration is that it cannot mathematically take into consideration changes in carbonate saturation state and should therefore only be applied to *O. umbonatus* Mg/Ca records where porewaters were well buffered (Lear et al., 2015). At Site 761, however, the downcore changes in Li/Ca ratios (Lear et al., 2010) suggest that the *O. umbonatus* specimens experienced changing $\Delta[CO_3^{2-}]$, likely due to slow sedimentation rates resulting in porewaters on the Wombat Plateau not being buffered to the same extent as elsewhere (Lear et al., 2015). For this reason, Lear et al. (2015) did not apply their calibration to the Mg/Ca data from Site 761. To circumvent this issue while employing the L2015 calibration, and thus a different seawater Mg/Ca value, we estimated the maximum likely bias caused by changes in porewater $\Delta[CO_3^{2-}]$. While core-top data confirm temperature as the dominant control on benthic foraminiferal Mg/Ca, they also estimate the offset caused by carbonate saturation state (Elderfield et al., 2006; Yu & Elderfield, 2008). Benthic foraminifera can be found in undersaturated bottom waters with $\Delta[CO_3^{2-}]$ as low as −20 μmol kg^{-1} (Elderfield et al., 2006). Above +25 μmol kg^{-1} any further change in $\Delta[CO_3^{2-}]$ has a negligible impact on Mg/Ca (Yu & Elderfield, 2008). Thus, we estimate a maximum $\Delta\Delta[CO_3^{2-}]$ of 45 μmol kg^{-1}. We follow Lear et al. (2010) in using the Mg/Ca-ΔCO_3^{2-} sensitivity of Elderfield et al. (2006) of 0.0086 mmol mol^{-1} per μmol kg^{-1},

allowing us to estimate a maximum potential bias of 0.4 mmol mol^{-1} (i.e., sensitivity multiplied by $\Delta\Delta[CO_3^{2-}]$). Using the average Mg/Ca value of the samples (~2.5 mmol mol^{-1}), the temperature bias is equivalent to ~1.4°C. Benthic foraminiferal Li/Ca suggests that $\Delta[CO_3^{2-}]$ at this site was generally lower in the Miocene Climatic Optimum than after the middle Miocene Climate Transition, and a marked minima in the sediment % coarse fraction suggests carbonate dissolution during the Miocene Climatic Optimum (Lear et al., 2010). We therefore suggest that the Mg/Ca temperatures calculated with the L2015 calibration might be biased towards cooler temperatures, particularly in the older portion of the record, by up to ~1.4°C.

Mg/Ca-based seawater $\delta^{18}O$ was calculated in the same manner as for Δ_{47}, using the $\delta^{18}O_b$ from Lear et al. (2010) of the same samples as the Mg/Ca analyses. The uncertainty of the Mg/Ca temperature was estimated following Lear et al. (2015). Those authors calculated a set of BWT time series, incorporating differences between Mg/Ca calibrations, a ± 0.5 mol/mol uncertainty in Mg/Ca$_{sw}$, and the range of values for B and H derived from the range of Mg/Ca$_{sw}$ assumed for the early Eocene period that their calibration is tied to (analytical uncertainty is very small in comparison, thus negligible). This set of temperature calculations results in a temperature envelope of approximately BWT $- 1.5$°C and BWT $+ 2.5$°C for the middle Miocene.

Uncertainty in Δ_{47} temperature is dominated by counting statistics associated with the analysis, with predictions of uncertainty based on mass spectrometer shot noise coming very close to our average analytical reproducibility (see Huntington et al., 2009, for further discussion). The latest improvements on Δ_{47} standardization routines have greatly improved inter-laboratory comparability and yield robust calibrations (Bernasconi et al., 2018; Meinicke et al., 2020). Thus, the major sources of error between the two proxies used here are very different, with uncertainty in Mg/Ca potentially controlled by systematic biases whereas Δ_{47} uncertainty is dominated by random error.

3. Results and Discussion

3.1. Species-Specific Effects on Δ_{47}

Grouping Δ_{47} values from multiple species together to generate one temperature estimate assumes the absence of species-specific effects. In modern core top samples, no species-specific effects have been found for benthic foraminifera outside the precision of the Δ_{47} thermometer (Grauel et al., 2013; Peral et al., 2018; Piasecki et al., 2019; Tripati et al., 2010). Here we compare multiple species downcore, for samples where temperatures are unknown, to assess whether our middle Miocene benthic foraminifera display the same lack of species-specific effect on Δ_{47}.

A one-way ANOVA was performed on our Δ_{47} data after dividing them into two groups: (1) older than 14.5 Ma and (2) younger than 13.5 Ma. This division is required to group the data into pools large enough to achieve a meaningful statistical power, and has the additional benefit that the shifting temperatures of the MCT cooling event, and less well replicated Δ_{47} values in that interval, are avoided. The results show no species-specific offsets (Figure 2), although an important caveat is that some species have not been analyzed in sufficient numbers ($n < 10$; only results for species with $n \geq 10$ are shown in Figure 2). Repeating the ANOVA with all data pooled together, we again observe no species-specific offsets, with the caveat that the data spread per species is slightly larger (not shown). Within current precision, our downcore comparison agrees with core top studies on the absence of species-specific effects on Δ_{47}. The lack of species-specific offsets on Δ_{47} indicates that pooling calcite from different species into single replicate measurements should not cause biases, which is particularly useful when material is sparse. However, nonlinear mixing, which occurs when stable isotope offsets between different constituents mixed into a single sample are large (Defliese & Lohmann, 2015), should still be considered; this effect is explained further in section 3.3.

3.2. Δ_{47} Temperature Results: Comparison of Averaging Methods

Figure 3 compares methods of calculating and presenting Δ_{47} temperatures using the described discrete binning or GWF (section 2.4) and compares these to the Mg/Ca-based temperature record. The results of the binning and smoothing methods are slightly different, although within uncertainty of each other.

For the GWF, window size and increment must be selected, both with units of time (Rodríguez-Sanz et al., 2017). A window as long as possible will reduce uncertainty, but the trade-off is that climate events can be smoothed out. Since the primary climate event of interest in this interval, the MCT, lasted for
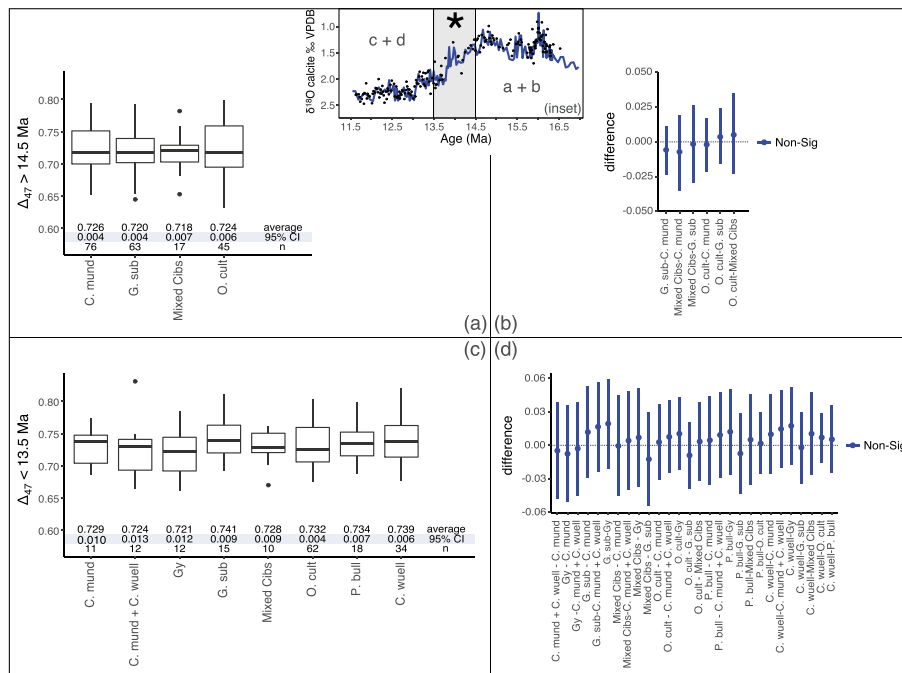
Figure 2. Statistical analysis of Δ_{47} results by species. Data were split into two groups, (a, b) >14.5 Ma and (c, d) <13.5 Ma, to avoid averaging over the strong change in $\delta^{18}O$ across the MCT (gray bar in inset) associated with temperature change. (a, c) Boxplots of Δ_{47} results by species; only those with $\geq$10 replicates are shown. (b, d) Results of one-way ANOVA with uncertainty calculated using Tukey's Honestly Different test indicating no interspecies offsets are apparent (significance at 95% CI). C. mund, *Cibicidoides mundulus*; C. wuell, *Cibicidoides wuellerstorfi*; Gy, *Gyroidinoides* spp; G. sub, *Globigerina subglobosa*; Mixed cibs, mixed *Cibicidoides* spp; O. cult, *Osangularia culter*; P. bull, *Pullenia bulloides*. (Inset) Published ODP Site 761 $\delta^{18}O$ records from Holbourn et al. (2004) and Lear et al. (2010) (line and points, respectively).

around 2 Ma, half this time (1 Myr) was selected. This selection is further justified by the fact that it ensures no fewer than 60 measurements are used per window. The step size of 100 ka was selected on the basis that, for the majority of the record, there are more than 10 new replicates per new temperature "window." An exception is the mid-MCT, where benthic foraminifera were scarce; uncertainty increases proportionally to reflect this scarcity of data (temporal distribution of Δ_{47} replicate measurements is shown in upper panels, Figure 3). The initial and final parts of the GWF curve were removed over the first/last 10 replicate measurements to avoid "edge effects." Other smoothing filters, using functions such as a cubed spline or locally weighted regression (LOESS/LOWESS), show similar but more pronounced edge effects; this is because the GWF results do not depend as strongly on data near the temporal end points of the record until much nearer those end points. Furthermore, other smoothing filters require selection of parameters such as degrees of freedom; in the case of this dataset, using an objective method such as generalized cross-validation to calculate degrees of freedom for a LOESS fit results in a nearly flat line across the record (not shown).

For the binning approach, the calculated mean temperatures are sensitive to the number of replicates used (Figures 3a–3c). As expected, the scatter of binned mean temperatures decreases with increasing replicates, and the bin means move closer to the values obtained with the smoothing function. The version we consider most robust is that with ~30 measurements per bin ($n = 27$–34), which yields 14 discreet temperature estimates (Figure 3c and supporting information). Due to the fact that individual temperature data points are each based on a large number of measurements, we calculate uncertainty from the sampling statistics of these data pools themselves (SE = 0.005 to 0.008‰) rather than using the long-term reproducibility of the secondary standard measurements (SE = 0.003 to 0.005‰).

The highest Δ_{47} temperature of 13.9 ± 3.8°C (95% CI) is observed at 16.2 Ma. While this apparently high temperature occurred close to the time of maximum CO_2 emissions from the Columbia River Basalt (Kasbohm & Schoene, 2018), its mean value falls outside the 68% CI uncertainty of the highest temperature calculated
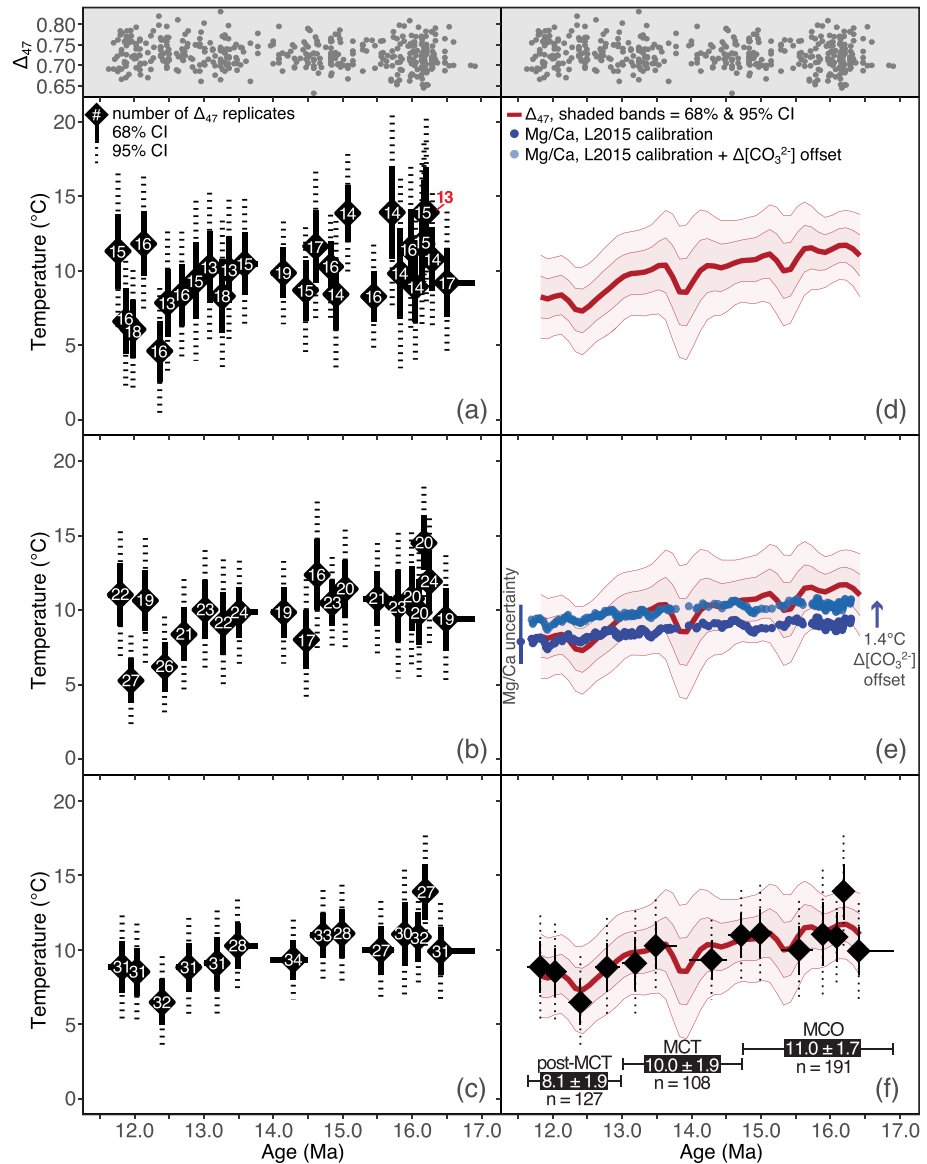
Figure 3. Comparison of different approaches for calculating temperature from individual Δ_{47} replicates and Mg/Ca-based temperatures. Discrete bins are shown as black diamonds with numbers of Δ_{47} measurements indicated in white (red number in (a) corresponds to a bin overlapped by another); horizontal bars indicate the age range of individual samples used for each bin. Gaussian Weighted Filter (GWF) shown as red line. Temperature uncertainty for both methods of calculating Δ_{47} temperature is given at the 68% and 95% confidence level, including calibration error. The preferred discrete bin size for this dataset is shown in (c) and (f), with $n = 27$–34. (e) The GWF Δ_{47} temperatures are compared to the Mg/Ca temperature record, both as calculated using L2015 and with the potential temperature offset due to changes in $\Delta[CO_3^{2-}]$. (f) Long-term discrete Δ_{47} temperature averages for MCO, MCT, and post-MCT ($\pm$ 95% CI), compared to the two versions of the Δ_{47} temperature record. Upper panels, temporal distribution of individual Δ_{47} measurements showing variations in data density.

using the GWF, $11.7 \pm 2.3°C$ (95% CI; Figures 3c and 3f; Table S2). Considering the uncertainty associated with our Δ_{47} temperatures, it would be prudent to attempt to replicate this temperature separately before this value is used as a constraint for past bottom water temperatures. The rest of the Δ_{47} temperatures calculated with the largest discrete bin size do not differ greatly from those calculated using the GWF; therefore, we focus on the GWF-based temperature record when comparing with the Mg/Ca-based temperatures in the following sections.
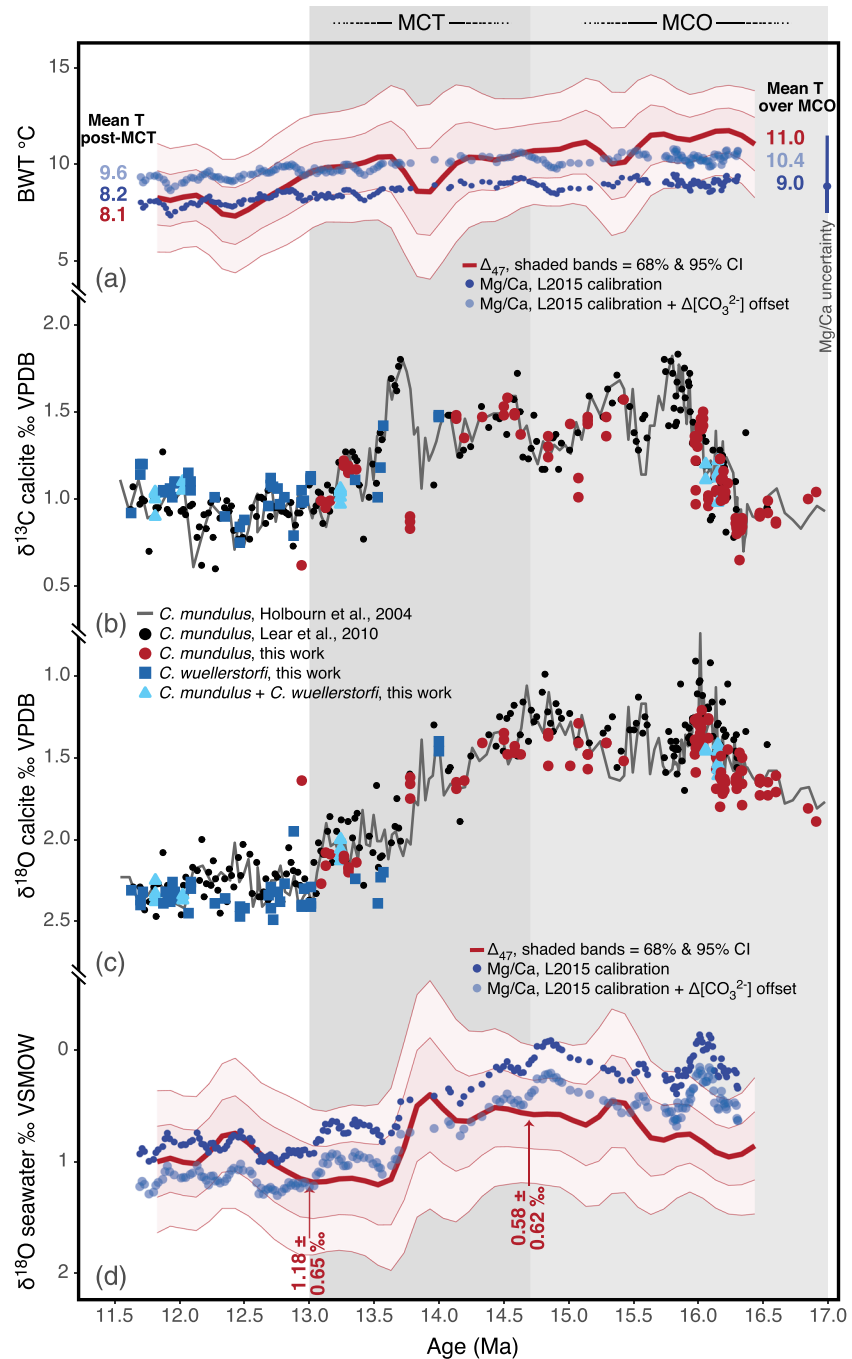
Figure 4. Comparison of climate records from the middle Miocene derived from Mg/Ca and Δ_{47}. (a) Bottom water temperatures (BWT) from Δ_{47} and Mg/Ca, either using the L2015 calibration or L2015 plus a possible offset due to $\Delta[CO_3^{2-}]$. Color-coded long-term average temperatures for the MCO and post-MCT sections for each proxy are shown for comparison. (b, c) Our new *Cibicidoides mundulus* and *Cibicidoides wuellerstorfi* $\delta^{18}O$ and $\delta^{13}C$ data (colored symbols) show no offsets to previously published records (black) (Holbourn et al., 2004; Lear et al., 2010). (d) Seawater $\delta^{18}O$ calculated from the temperature records in (a).

3.3. Δ_{47} Temperature Results and Comparison to Mg/Ca Temperatures

In the following, the ages used to define the MCO, MCT, and post-MCT climate "regimes" are defined by changes in the $\delta^{18}O_b$ record (Figure 4c). Our new stable isotope data are essentially indistinguishable from independently generated records (Figures 4b and 4c; Holbourn et al., 2004; Lear et al., 2010). We use the

Table 1

Comparison of Long-Term Bottom Water Temperatures and $\delta^{18}O_{sw}$ at ODP Site 761 Derived From Δ_{47} and the Different Mg/Ca Methods Discussed in the Text

	Δ_{47}		Mg/Ca	
Climate regime[a]	Discrete bins[b]	GWF[c]	L2015	L2015 + 1.4°C
		Temperature (°C)		
Δ across MCT	2.9 ± 2.5	2.9 ± 4.0	0.8[d]	0.8[d]
Post-MCT	8.1 ± 1.9	8.2 ± 2.8	8.2	9.6
MCT	10.0 ± 1.9	9.9 ± 3.4	8.7	10.1
MCO	11.0 ± 1.7	11.0 ± 2.8	9.0	10.4
		$\delta^{18}O_{sw}$ (‰ VSMOW)		
Δ across MCT	0.36 ± 1.0	0.64 ± 0.88	0.83[e]	0.84[e]
13.0 Ma	1.01 ± 0.80	1.18 ± 0.65	0.93	1.24
14.7 Ma	0.65 ± 0.66	0.54 ± 0.59	0.10	0.40

[a]Ages of long term bins: post-MCO < 13.0 Ma < MCT < 14.7 Ma < MCO. See text for justification. [b]Discrete bin uncertainties 95% CI. [c]Note that the long-term discrete bin and GWF temperature uncertainties in this table are not calculated in an identical matter. Long-term GWF temperature uncertainties are an average of the 95% confidence intervals in the respective time interval, whereas the discrete bin uncertainties are the 95% CI based on the distribution of all individual Δ_{47} values. The calculation was performed on the GWF values in this way to provide a better comparison (rather than with an artificially small uncertainty caused by using a pre-smoothed sample pool). [d]Values likely an underestimate due to the changing $\Delta[CO_3^{2-}]$ bias exerted on Mg/Ca across the record; see sections 2.5, 3.3, and 3.4 for details. [e]Values likely an overestimate due to the changing $\Delta[CO_3^{2-}]$ bias exerted on Mg/Ca across the record; see sections 2.5, 3.3, and 3.4 for details.

inflection points on the composite dataset to define the intervals. The MCT is defined as the region between 13.0 and 14.7 Ma; all data older than this interval are considered to fall into the MCO, and all data younger than this interval are classified as post-MCT. These ages bracket the major MCT ice sheet advances between 14.7 and 13.8 Ma (Levy et al., 2016). Bracketing the MCT in this manner also allows us to consider climate mean states before and after the MCT.

Our GWF-calculated Δ_{47} temperature record indicates a range of bottom water temperatures over the MCO from 10.0 ± 3.6°C to 11.7 ± 2.3°C, with an overall average of 11.0°C (Figures 3 and 4 and supporting information). Averaging all individual Δ_{47} measurements across the entire MCO gives a value of 11.0 ± 1.7°C (Table 1 and Figure 3f), identical to the average GWF result. In the post-MCT interval, the GWF-calculated Δ_{47} temperatures range between 7.3 ± 2.9°C at 12.4 Ma to 9.3 ± 3.1°C at 12.9 Ma, with an overall average of 8.2 ± 2.8°C. The GWF-based average again compares very well to the discrete bin average of all post-MCT measurements of 8.1 ± 1.9°C. These values suggest the overall cooling over the transition was 2.9 ± 2.5°C. A two-sample *t* test shows that the long-term discrete bin average Δ_{47} values of the post-MCT and MCO periods are significantly different ($p < 0.005$), lending confidence to this estimate.

The Δ_{47} temperatures agree very well with the Mg/Ca temperatures, with the L2015 based record and the version of this record including the potential $\Delta[CO_3^{2-}]$ offset both being within the 68% CI band over the majority of the record (Figures 3e and 4a). This result is unexpected considering the uncertainty relating to the important seawater chemistry parameters necessary to calculate absolute temperature from foraminiferal Mg/Ca such as seawater Mg/Ca and the uncertainties associated with the Mg/Ca sensitivity to $\Delta[CO_3^{2-}]$ discussed above (section 2.5). Though still within uncertainty, the Mg/Ca-based ΔT across the MCT is low relative to the mean Δ_{47}-based ΔT for the same interval. As stated in section 2.5, it is likely that the $\Delta[CO_3^{2-}]$ effect on Mg/Ca was higher in the MCO, suggesting the change in BWT of 0.8°C is an underestimate. The fact that the offset between the proxies is most pronounced during the MCO, a time when $\Delta[CO_3^{2-}]$ is expected to have been most impacted by relatively high atmospheric CO_2, indicates that changes in carbonate saturation state are the most likely explanation of the offset. The direction of the offset suggests that the Mg/Ca temperatures could be depressed relative to the rest of the record during that time.

The remaining question to explore is whether these relatively warm temperatures, as estimated by both proxies, are realistic. They seem hard to reconcile with evidence for significant ice volume on the Antarctic continent and atmospheric CO_2 concentrations between modern and preindustrial levels (Sosdian et al., 2018; Super et al., 2018) after the MCT. These temperatures also lead to the calculation of
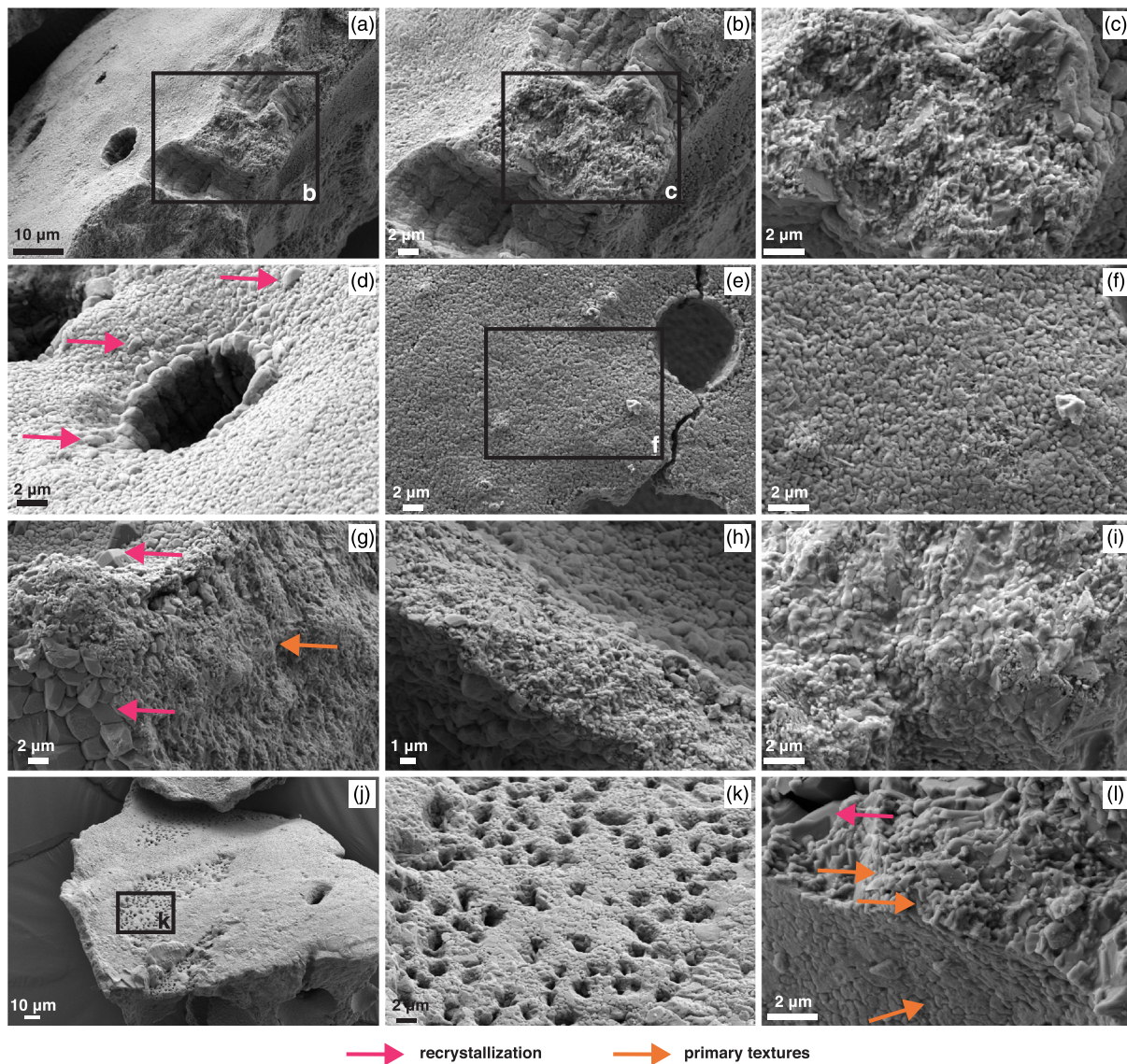
Figure 5. Scanning electron micrographs of representative cracked and cleaned *Cibicidoides mundulus* (a–i) and *Osangularia culter* (j–l). (a–c) Pore canals lined by euhedral calcite crystals arranged in layers suggesting organic control; test wall cross section texture suggests limited if any recrystallization to internal material. (d–f) Outer test surfaces show a range of recrystallization extent; blocky calcite crystals are more common on some tests (magenta arrows, d, g) compared to others (e, f). (g–i) A range of test wall cross sections showing extensive recrystallization on exposed surfaces but little to no recrystallization of internal calcite. (m–o) *O. culter* specimens with moderate recrystallization on outer surfaces (j, k) compared to less recrystallization on internal test chamber surfaces and cross sections (l). Samples shown are fragments of tests derived from cracked and cleaned foraminifera taken from sample batches used for clumped isotope analysis. Samples: (a, b, c, e, f, i) ODP 761B 06-02 53-55; (d, h) ODP 761B 06-04 83-85; (h) ODP 761B 06-02 98-100; (j, k) ODP 761B 05-05 113-115; and (l) ODP 761B 06-03 58-60.

heavy seawater $\delta^{18}O$ (discussed further in section 3.4). For Δ_{47}, biases may be caused by thermal and non-thermal factors, including incorporation of calcite formed at the sea surface (e.g., coccoliths) and recrystallization of primary calcite at warmer temperatures. Recrystallization of primary calcite to highly offset stable isotope compositions, even if it occurred at the same temperature as primary calcification, could also cause bias due to nonlinear mixing effects.

While a few nannofossil remnants are visible in some SEM images, a conservative estimate is that they make up far less than 1% of the material analyzed, and they should therefore not impart a measurable bias. However, most specimens seem to display some degree of recrystallization (Figures 5 and 6); thus, the effects of this process must be considered. The main observations from our SEM images are (1) exposed surfaces of
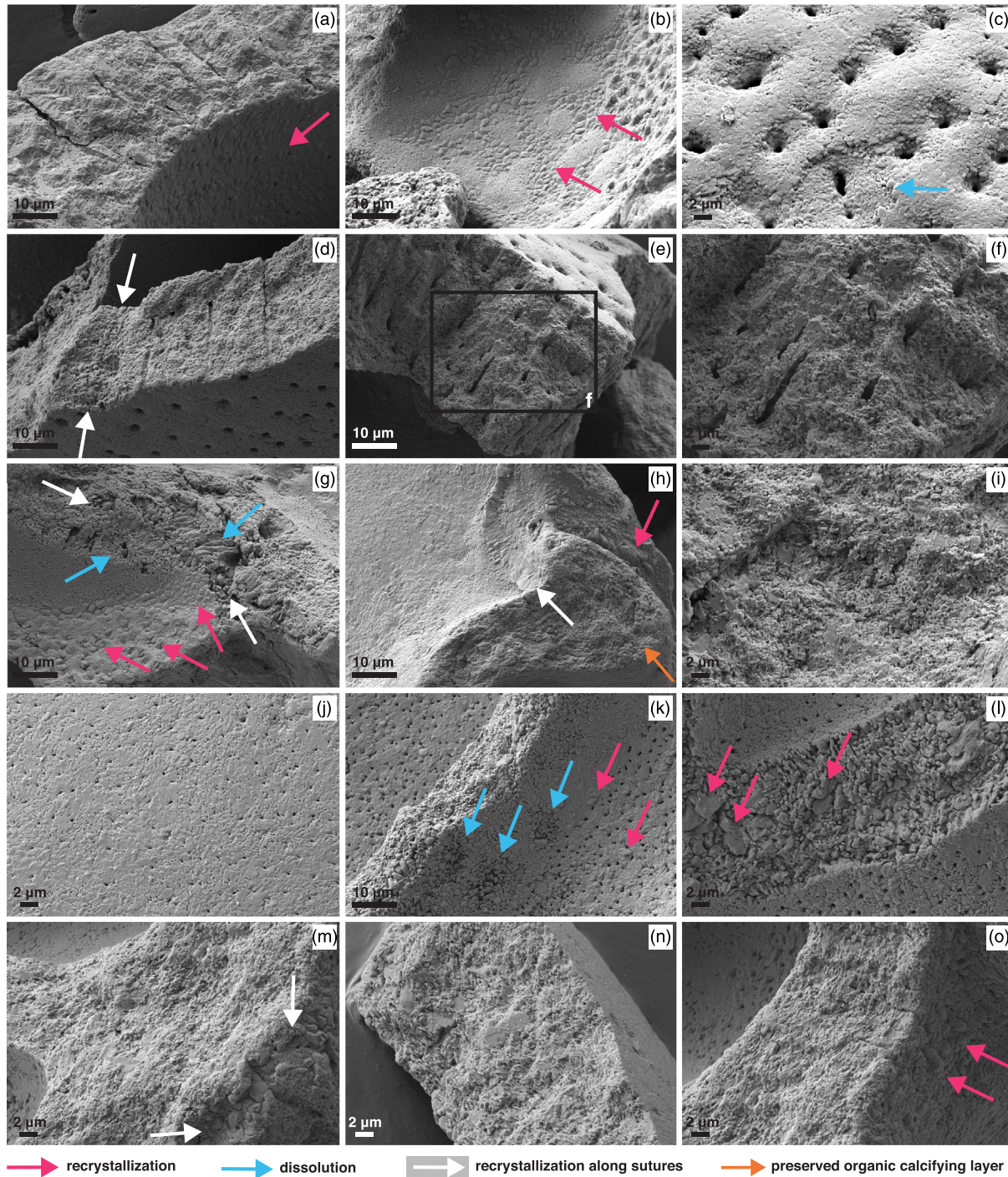
Figure 6. Scanning electron micrographs of representative cracked and cleaned *Globocassidulina subglobosa* (a–i) and *Gyroidinoides* spp (j–o). (a, b) Recrystallization on interior chamber surfaces. (c) Representative surface texture with preserved pore canals, showing some dissolution. (d–f) Pore canals are well preserved. (d, g, h) Sutures are sometimes associated with discrete layers of euhedral recrystallized calcite in *G. subglobosa* samples. (h) Some organic calcifying layer structures are preserved (orange arrow), and (i) some samples do not exhibit recrystallization in cross section. (j) Typical external surface texture in *Gyroidinoides* spp, with few obviously recrystallized features. (k–o) *Gyroidinoides* exhibit more blocky calcite in test wall cross section than other species examined in this study, as well as varying degrees of dissolution (k) and internal chamber surface recrystallization (o). Samples shown are fragments of tests derived from cracked and cleaned foraminifera taken from sample batches used for clumped isotope analysis. Samples: (a, b, g, h) ODP 761B 05-04 18-20; (c, e, f, i) ODP 761B 06-02 3-5; (d) ODP 761B 06-02 53-55; (j–o) ODP 761B 06-01 58-60.

test walls tend to exhibit blocky, euhedral inorganic calcite, varying from a few crystals across an entire test to large areas of the surfaces being recrystallized, and (2) cross sections through freshly broken test walls exhibit what appear to be primary textures alongside textures associated with inorganic crystallization in highly varying proportions. These observations indicate that the primary calcite is mixed with recrystallized calcite to varying degrees in our samples. However, benthic foraminifera are thought to undergo most recrystallization relatively early during burial (Edgar et al., 2013; Leutert et al., 2019; Voigt et al., 2015, 2016). Even if some recrystallization occurred at a later stage during burial, our samples were relatively shallowly buried (~35 to 52 mbsf), leading to negligible geothermal heating at burial depth. The geothermal gradient effect would furthermore have been counteracted by deep-water cooling over the period since deposition. Consequently, it is unlikely that recrystallization occurred under a significantly different temperature regime. If recrystallization did occur much later than deposition, due to the shallow burial depth, the Δ_{47} compositions would most likely be biased towards lower temperatures, but this cannot explain the offset to slightly warmer temperatures compared to the Mg/Ca values.

Nonlinear mixing effects can cause a warm or cold bias beyond analytical precision if both the $\delta^{13}C$ and $\delta^{18}O$ compositions of the recrystallized material are more than 2‰ offset from the primary calcite (the required difference increases to ~15‰ if only one of $\delta^{13}C$ or $\delta^{18}O$ is offset; Defliese & Lohmann, 2015). We consider such different composition of the diagenetic calcite phase as highly unlikely. The recrystallized portion of material could potentially have much different $\delta^{13}C$ or $\delta^{18}O$ if calcification occurred in a fluid influenced by dissolved inorganic carbon (DIC) or other sediment components with very different isotopic compositions. However, Site 761 sediments are carbonate-rich and low in total organic carbon (TOC) in the studied interval (~81% to 92% $CaCO_3$, ≤0.02% TOC; Shipboard Scientific Party, 1990), indicating no significant influence on pore fluid DIC from organic material (normally characterized by isotopically light carbon). Similarly carbonate-rich sites show minimal isotopic offsets in benthic foraminifera regardless of the amount of recrystallization (Voigt et al., 2016). Furthermore, the $\delta^{13}C$ and $\delta^{18}O$ values of *C. mundulus* and *C. wuellerstorfi* from Site 761 are very similar in absolute values, trends, and magnitude of change to records produced from similar benthic species at a wide array of pelagic sites (including, but not limited to, Eastern Pacific Sites 1236 and 1237, Holbourn et al., 2013, and Sites U1335, U1336, U1337, and U1338, Kochhann et al., 2016; Southern Ocean/Tasmanian Gateway Site 1171, Shevenell & Kennett, 2004; and Southwest Pacific Site 588A, Flower & Kennett, 1995). If post-depositional diagenetic overprinting due to the local carbon and oxygen pools had caused offsets in the stable isotope composition of the recrystallized material, it is unlikely that our stable isotope data would agree so well with such a far-reaching array of co-eval benthic foraminifera records. Our findings are consistent with the recent study of Leutert et al. (2019), which determined that benthic foraminiferal Δ_{47} compositions are largely robust to diagenesis in typical deep-sea settings.

For Δ_{47} compositions, a final mechanism to consider is the effect of dissolution; unfortunately, its effects have not yet been tested. Although we observe some dissolution of foraminiferal calcite in the SEM images (Figure 6), this does not appear to be particularly extensive, nor does it seem to occur to different extents in different time intervals. Changes in the percent coarse fraction and changes in sedimentation rate, two variables which could be related to dissolution, do not appear related to the Δ_{47} temperatures (Figure S2). Thus, while a dissolution effect cannot be ruled out, dissolution itself appears to have occurred to a minor degree in our samples.

The primary potential causes for biases in Mg/Ca temperatures include incorrect assumptions regarding the species-specific temperature calibration or seawater Mg/Ca values used, changes in carbonate saturation state, and diagenetic addition of Mg. Salinity and pH effects are not discussed here as these have not been shown to have an effect on benthic foraminifera. Middle Miocene seawater Mg/Ca composition is fairly uncertain (see Figure 2 of Evans, Sagoo, et al., 2018; Figure 5 of Lear et al., 2015; and Figure 9 of Tierney et al., 2019). However, the species used for Mg/Ca analysis at Site 761 (*O. umbonatus*) is thought to be relatively insensitive to changes in seawater Mg/Ca (H = 0.27 ± 0.06; Lear et al., 2015). Even considering a range of sensitivities to this parameter combined with a range of seawater Mg/Ca values, the upper range of the estimated Mg/Ca uncertainty does not expand beyond the upper 68% CI band of the Δ_{47} temperatures for most of the record.

Compared to a coeval section at Pacific Ocean ODP Site 806, Lear et al. (2015) noted that Site 761 samples had elevated Mn/Ca and higher Mg/Ca ratios. Those authors concluded that the observed Mg/Ca offset

was caused either by porewater carbonate saturation effects or diagenetic contamination, the latter implying a warm bias in the Mg/Ca temperatures at ODP Site 761. This is important because, as indicated above, Site 761 exhibits unusual porewater chemistry, with possible consequences for Mg/Ca in the shallow infaunal *O. umbonatus*. The [Mg] porewater profile at Site 761 is monotonous over the upper 300 m of sediment, rather than decreasing as observed at other pelagic sites (De Carlo, 1992). It is thought that this unusual profile is due to the shallow burial and low level of lithification allowing seawater circulation through the pore space to a higher degree than at other pelagic marine sites (De Carlo, 1992), leading to a lack of effective buffering capacity. Though the two proxies used here produce temperatures generally within uncertainty, the long-term trend of the Mg/Ca temperatures follows a much shallower slope (Figures 3 and 4), also illustrated by the smaller ΔT between the MCO and post-MCT periods compared to the Δ_{47}-based temperatures (Table 1). The difference in ΔT, and apparently larger difference between Δ_{47} and Mg/Ca based temperatures in the MCO, implies that carbonate saturation effects may bias the Mg/Ca record towards colder temperatures in this interval, supporting the interpretation of Lear et al. (2010). While the uncertainty of Δ_{47} does not allow us to conclude with confidence, the $\Delta[CO_3^{2-}]$ corrected Mg/Ca temperatures are closer to the average Δ_{47} temperatures in the MCO. Changes in carbonate saturation state are not thought to affect carbonate Δ_{47} compositions to a measurable extent (Eagle et al., 2013; Hill et al., 2014; Kelson et al., 2017; Tang et al., 2014; Tripati et al., 2015).

When comparing the absolute temperatures, the effect of diagenesis on benthic foraminiferal Mg/Ca should also be considered. If the inorganic Mg partition coefficient is higher than the foraminiferal Mg partition coefficient, recrystallisation of primary calcite or addition of inorganic calcite could be expected to result in a bias to warmer temperatures. Though this argument has been invoked previously (e.g., Bryan & Marchitto, 2008), electron microprobe analyses have recently shown that the difference between the Mg partition coefficients for benthic foraminiferal calcite and inorganic calcite is likely orders of magnitude smaller than previously thought, at least for the natural range of ocean bottom water temperatures (Lammers & Mitnick, 2019). Nevertheless, it is thought that biological control during calcification limits Mg^{2+} incorporation into foraminiferal calcite (e.g., Bentov & Erez, 2006). High-resolution secondary ion mass spectrometry results from Kozdon et al. (2013) seem to support a middle ground between these arguments, showing an approximate doubling of the Mg/Ca ratio in inorganic overgrowths on planktic foraminifera compared to primary material. While even a doubling of Mg/Ca in any inorganic calcite overgrowths would undoubtedly impact the calculated temperatures, we do not observe significant inorganic calcite overgrowths on our specimens of the type investigated by Kozdon et al. (2013) (Figures 5 and 6). If our samples were affected by significant proportions of calcite overgrowths, we would also expect the Mg/Ca and Δ_{47} temperatures to diverge more, since the effect on each proxy would be opposite (warmer apparent temperatures in the case of Mg/Ca, the same or cooler in the case of Δ_{47}).

While we have discussed potential biases at length, it is important to highlight how well the two proxy temperature records agree overall. The Mg/Ca and Δ_{47} thermometers suffer from different potential biases, often working in opposite directions. This is particularly important considering the relatively poor constraints on Miocene seawater Mg/Ca and carbonate saturation state changes and their effect on Mg/Ca temperatures, as well as any as-yet unknown effects due to dissolution or unaccounted for diagenetic effects which could bias the Δ_{47} temperature record. Consequently, the similarity between the Mg/Ca and Δ_{47} temperature estimates at ODP Site 761 lends credibility to the finding that deep ocean temperatures here were significantly warmer than today across the entire interval from 16.5–11.5 Ma. The Δ_{47}-based temperatures of 11°C during the MCO and 8°C post-MCT are about 9°C and 6°C warmer than present, respectively, for bottom waters at Site 761. Mg/Ca-based temperatures, whether corrected for the carbonate saturation state effect or not, agree very well, particularly in the younger part of our record. While high CO_2 concentrations are invoked for the relative warmth of the MCO, the post-MCT period is characterized by atmospheric CO_2 concentrations on average somewhere between pre-industrial and modern (between 280 and 400 ppm; Sosdian et al., 2018; Super et al., 2018), suggesting a significantly different climate state for similar greenhouse forcing.

3.4. Seawater δ^{18}O

The GWF Δ_{47}-based $\delta^{18}O_{sw}$ record shows relatively heavy values, averaging approximately 0.5‰ during the MCO and approximately 1‰ after the MCT. Before and during the MCT, the Δ_{47}-based $\delta^{18}O_{sw}$ values are slightly higher than those derived using Mg/Ca temperatures (Figure 4d), a result of the combination of

slightly warmer mean temperatures, particularly when not correcting for the carbonate saturation state effect, and essentially identical $\delta^{18}O_b$ (Figure 4c). Mg/Ca-based $\delta^{18}O_{sw}$ was calculated using the $\delta^{18}O_b$ from the same samples as presented in Lear et al. (2010), whereas Δ_{47}-based $\delta^{18}O_{sw}$ is calculated using our new $\delta^{18}O_b$ measurements. As our new stable isotope compositions do not show any offsets compared to two independently generated records (Figures 4b and 4c; Holbourn et al., 2004; Lear et al., 2010), the two $\delta^{18}O_{sw}$ records are comparable.

To estimate the change in $\delta^{18}O_{sw}$ across the MCT, we use the $\delta^{18}O_{sw}$ values from GWF windows centered around time slices at the onset and end of the MCT (13.0 and 14.7 Ma; values marked with red arrows in Figure 4d) rather than the long-term average values discussed above for temperature. This approach allows us to avoid the less-well replicated section in the center of the MCT and be more comparable to other records focusing solely on the transition. Δ_{47}-based $\delta^{18}O_{sw}$ values at the beginning and end of the MCT ($0.54 \pm 0.59‰$ at 14.7 Ma and $1.18 \pm 0.65‰$ at 13.0 Ma) suggest an increase of $0.64 \pm 0.88‰$ across the transition. These estimates are only very weakly dependent on the poorly replicated region between 13.4 and 13.9 Ma, and the Δ_{47}-based $\delta^{18}O_{sw}$ record is fairly consistent across the early and late parts of the MCT interval, indicating this value of relative change over the climate transition is robust. The Mg/Ca-based change in $\delta^{18}O_{sw}$ across the MCT of about 0.8‰ is within uncertainty of that derived from Δ_{47}, although this is likely overestimated considering the Li/Ca evidence for changes in saturation state. This estimate does not take into consideration that a $\Delta[CO_3^{2-}]$ bias correction is likely appropriate in the older part of the Mg/Ca record, particularly the MCO, whereas it may be unnecessary to make this correction in the youngest part of the record. Lear et al. (2010) suggested that a change in $\delta^{18}O_{sw}$ of 0.6‰ was most accurate based on the combined Mg/Ca and Li/Ca data, which is nearly identical to our Δ_{47}-based seawater $\delta^{18}O$ estimate.

Taken at face value, the Δ_{47} $\delta^{18}O_{sw}$ record suggests ~73% of the change in $\delta^{18}O_b$ at Site 761 is due to increased ice volume. This estimate is consistent with Mg/Ca-based estimates at other sites (e.g., ~70% at ODP Site 1171, Shevenell et al., 2008; $60 \pm 14\%$ from a global meta-analysis by Mudelsee et al., 2014). It is also consistent with the fact that the $\delta^{18}O_b$ record of Site 761 closely follows the global sea level curve between ~15.1 and 11.5 Ma (Holbourn et al., 2004), which implies that the deep water at ODP Site 761 tracked global climate signals.

Compared to modern $\delta^{18}O_{sw}$, both Δ_{47} and Mg/Ca-based $\delta^{18}O_{sw}$ estimates suggest that $\delta^{18}O_{sw}$ values were relatively high across the record and significantly higher than present after the MCT, reaching similar values to those observed for the last glacial maximum (LGM). This observation, if interpreted in terms of ice volume, is difficult to reconcile with the significantly warmer than modern bottom water temperatures suggested by both proxies, as well as our current theories of global mean sea level for the middle Miocene. Our assessment of potential nonthermal biases of the proxies does not support a diagenetic control on temperature and thus $\delta^{18}O_{sw}$, although we acknowledge that there may be other unknown biases that we have not accounted for.

If these high $\delta^{18}O_{sw}$ values are accurate, they may imply either a larger than modern global ice volume after the MCT, a strongly different isotopic composition of the ice sheet during this time period, and/or that high salinity (and correspondingly high $\delta^{18}O_{sw}$) bottom waters were more persistent in the deep oceans, as suggested for tropical Pacific ODP Site 806 (Lear et al., 2015). Our heavy values could also reflect the effects of different seawater pH on $\delta^{18}O_b$ (Zeebe, 1999) or possibly different species-specific $\delta^{18}O$ fractionation during calcification (vital effects) compared to today. The latter effects are difficult to test quantitatively. Although distinct relationships between calcite $\delta^{18}O$ and pH have been found for planktic species (Spero et al., 1997; Uchikawa & Zeebe, 2010), Marchitto et al. (2014) did not find a clear relationship between pH and the calcite $\delta^{18}O$ of the epifaunal benthic species that make up a large part of our record. It is also impossible to directly test living specimens to examine whether vital effects were different during the middle Miocene compared to today.

Storage of water on the poles, in ice or otherwise, could explain a large part of the difference between our expectations and our results if conditions were different to today. Evidence is insufficient to support significant ice in the Northern Hemisphere during the middle Miocene (Larsen et al., 1994); thus, storage within ice sheets was likely primarily restricted to Antarctica. It is possible that the topography of Antarctica was different in the middle Miocene, such that the area available for ice growth could have been larger (e.g., Gasson et al., 2016), and there is geomorphological evidence for ice sheets which were

significantly thicker than today (Denton et al., 1984; Denton & Sugden, 2005). Ice grounding lines extending significantly further than modern also suggest larger than modern ice sheet extent (e.g., Passchier et al., 2011). Recently, it has also been suggested that during deeper geological time periods such as the Cenomanian and Turonian hothouse periods, groundwater storage must be invoked to account for sea level cycles in an ice-free world (Sames et al., 2020).

In addition to a different volume of water stored on land, the isotopic difference between the deep ocean and terrestrial water storage reservoirs could have been greater than today. Thicker ice sheets covering a smaller area, positioned far from the source of evaporation, could at least partly address the issue, since both longer distances and higher elevations would drive the necessary fractionation. However, it is highly improbable that this latter possibility is the sole explanation for the heavy $\delta^{18}O_{sw}$; assuming the same sea level and ice volume as today, an average "stored water" $\delta^{18}O$ of $-70‰$ would only explain a $0.3‰$ difference in seawater $\delta^{18}O$ (compare to modern $\delta^{18}O$ values in Greenland ice [$\sim-35‰$] and Antarctic ice [$\sim-55‰$]).

Finally, our heavy $\delta^{18}O_{sw}$ results could be explained by a different source of deep waters, specifically a process which produced more saline and correspondingly heavier $\delta^{18}O$ deep waters. Evaporation-dominated deep water formation would provide the necessary mechanism, though there is little evidence available for where and how this mechanism might have operated for the middle Miocene. Relatively heavy $\delta^{18}O_b$ values from a suite of ODP Sites have previously been explained as resulting from evaporation-controlled saline deep water derived from the Tethys Ocean, although the water mass responsible is thought to have ceased by ~14.5 Ma (Ramsay et al., 1998). Woodruff and Savin (1989) envisioned a scenario in which this water mass could have been refrigerated as it moved southwards and was re-entrained in high latitude deep water formation; this might explain the temperatures we have reconstructed being inconsistent with tropical or subtropical latitude deep water formation.

The discussion above indicates a middle Miocene $\delta^{18}O_{sw}$ paradox, suggesting that deep water $\delta^{18}O_{sw}$ values cannot be explained with our current understanding of the primary controls on seawater $\delta^{18}O$. The very good agreement between the Mg/Ca- and Δ_{47}-derived temperatures at Indian Ocean Site 761 provides confidence that these high seawater $\delta^{18}O$ values are accurate. Benthic records from western equatorial Pacific ODP Site 806 and Southern Ocean ODP Site 1171 have independently produced similarly high bottom water $\delta^{18}O_{sw}$ values for the post-MCT period (Lear et al., 2015; Shevenell et al., 2008), consistent with our assessment. These records are based on benthic foraminiferal Mg/Ca, but use different species (epifaunal *C. mundulus* in the case of Site 1171) or are based on the same species (*O. umbonatus*) but from porewater which was likely buffered against changes in the carbonate saturation state (Pacific ODP Site 806). The consistency of these findings taken together suggests gaps in our understanding of the warmer middle Miocene climate system and should be explored further in future work. In particular, oxygen isotope-enabled modeling could greatly enable more insight into this apparent paradox.

4. Conclusions

We applied clumped isotope thermometry to benthic foraminifera across the middle Miocene climate transition. Reconstructed temperatures are based on a large number of measurements on multiple species from multiple downcore samples. In agreement with previous core top studies, our downcore Δ_{47} results show no indication of species-specific effects on benthic foraminiferal Δ_{47} compositions. A moving average smoothing function such as the probabilistic Gaussian Window Filter (GWF) first proposed for Δ_{47} data by Rodríguez-Sanz et al. (2017) yields a robust temperature record for Site ODP 761.

The long-term discrete average Δ_{47} temperatures calculated for the MCO ($11.0 \pm 1.7°C$) and post-MCT ($8.1 \pm 1.9°C$) are statistically distinguishable and suggest a cooling across the MCT of approximately $2.9 \pm 2.5°C$.

Our bottom water Δ_{47} temperature record agrees well with temperatures based on previously published Mg/Ca ratios, whether these are corrected for an offset caused by the carbonate saturation state effect on benthic foraminiferal Mg/Ca or not. Larger apparent offsets between the two proxies during the earlier (MCO) part of the record confirm previously suggested saturation state effects on Mg/Ca in that interval. Although we cannot completely rule out diagenesis-related biases in Δ_{47} or Mg/Ca, the most likely effects of post-depositional recrystallisation would work in opposite directions for the two proxies and are not

supported by the slight positive offset of Δ_{47} compared to the Mg/Ca temperatures in parts of the record. Considering that seawater Mg/Ca and changes in saturation state are poorly known quantities which may affect Mg/Ca based temperatures, while the effects of dissolution on Δ_{47} are currently unconstrained, the agreement between the two proxies is remarkably good.

The Δ_{47} thermometer estimates a change in $\delta^{18}O_{sw}$ of ~0.6‰ across the MCT, in excellent agreement with the Mg/Ca paleothermometer (Lear et al., 2010). The Δ_{47}-based estimate is also consistent with other estimates of $\delta^{18}O_{sw}$ change over this interval. As previously observed, $\delta^{18}O_{sw}$ values are relatively heavy throughout the record, resulting in post-MCT values similar to those reconstructed for the last glacial maximum. For the reconstructed values to be realistic, we discuss several options, which in part appear to be contradictory to the warm bottom water temperatures we observe for the middle Miocene. This suggests that the middle Miocene relationship between $\delta^{18}O_{sw}$ and ice volume was different from the present or more recent glacial periods and requires further research.

While currently the Δ_{47} proxy requires substantial amounts of sample material (2–3 mg), it is not affected by changes in seawater chemistry and species-specific offsets. Mg/Ca is capable of providing temperature information at significantly higher temporal resolution due to the smaller sample mass requirements, but can be biased by a range of factors which become more poorly constrained further back in time. Thus, these two proxies are highly complementary and lend themselves well to a multiproxy approach. In this case, the comparison of Δ_{47}- and Mg/Ca-based records has provided more confidence in the warm bottom water temperatures estimated at ODP Site 761 during the middle Miocene.

Data Availability Statement

All data related to this study can be found in the supporting information (standard results and final calculated temperatures) as well as in two online repositories. Raw data are available in the EarthChem Database (https://doi.org/10.26022/IEDA/111523); final calculated temperatures are available at Pangaea (https://doi.pangaea.de/10.1594/PANGAEA.914305).

Conflict of Interest

The authors declare no conflicts of interest relevant to this study.

References

Affek, H. P., Bar-Matthews, M., Ayalon, A., Matthews, A., & Eiler, J. M. (2008). Glacial/interglacial temperature variations in Soreq cave speleothems as recorded by "clumped isotope" thermometry. *Geochimica et Cosmochimica Acta*, *72*(22), 5351–5360. https://doi.org/10.1016/j.gca.2008.06.031

Badger, M. P. S., Lear, C. H., Pancost, R. D., Foster, G. L., Bailey, T. R., Leng, M. J., & Abels, H. A. (2013). CO_2 drawdown following the middle Miocene expansion of the Antarctic Ice Sheet. *Paleoceanography*, *28*(1), 42–53. https://doi.org/10.1002/palo.20015

Barker, S., Greaves, M., & Elderfield, H. (2003). A study of cleaning procedures used for foraminiferal Mg/Ca paleothermometry. *Geochemistry, Geophysics, Geosystems*, *4*, 1–20. https://doi.org/10.1029/2003GC000559

Bentov, S., & Erez, J. (2006). Impact of biomineralization processes on the Mg content of foraminiferal shells: A biological perspective. *Geochemistry, Geophysics, Geosystems*, *7*, Q01P08. https://doi.org/10.1029/2005GC001015

Bernasconi, S. M., Hu, B., Wacker, U., Fiebig, J., Breitenbach, S. F. M., & Rutz, T. (2013). Background effects on Faraday collectors in gas-source mass spectrometry and implications for clumped isotope measurements. *Rapid Communications in Mass Spectrometry*, *27*(5), 603–612. https://doi.org/10.1002/rcm.6490

Bernasconi, S. M., Müller, I. A., Bergmann, K. D., Breitenbach, S. F. M., Fernandez, A., Hodell, D. A., et al. (2018). Reducing uncertainties in carbonate clumped isotope analysis through consistent carbonate-based standardization. *Geochemistry, Geophysics, Geosystems*, *19*, 2895–2914. https://doi.org/10.1029/2017GC007385

Billups, K., & Schrag, D. P. (2003). Application of benthic foraminiferal Mg/Ca ratios to questions of Cenozoic climate change. *Earth and Planetary Science Letters*, *209*(1–2), 181–195. https://doi.org/10.1016/S0012-821X(03)00067-0

Bonifacie, M., Calmels, D., Eiler, J. M., Horita, J., Chaduteau, C., Vasconcelos, C., et al. (2017). Calibration of the dolomite clumped isotope thermometer from 25 to 350°C, and implications for a universal calibration for all (Ca, Mg, Fe)CO_3 carbonates. *Geochimica et Cosmochimica Acta*, *200*, 255–279. https://doi.org/10.1016/j.gca.2016.11.028

Brand, W. A., Assonov, S. S., & Coplen, T. B. (2010). Correction for the ^{17}O interference in $\delta(^{13}C)$ measurements when analyzing CO_2 with stable isotope mass spectrometry (IUPAC Technical Report). *Pure and Applied Chemistry*, *82*(8), 1719–1733. https://doi.org/10.1351/PAC-REP-09-01-05

Breitenbach, S. F. M., Mleneck-Vautravers, M. J., Grauel, A. L., Lo, L., Bernasconi, S. M., Müller, I. A., et al. (2018). Coupled Mg/Ca and clumped isotope analyses of foraminifera provide consistent water temperatures. *Geochimica et Cosmochimica Acta*, *236*, 283–296. https://doi.org/10.1016/j.gca.2018.03.010

Broecker, W., & Yu, J. (2011). What do we know about the evolution of Mg to Ca ratios in seawater? *Paleoceanography*, *26*, 1–8. https://doi.org/10.1029/2011PA002120

Bryan, S. P., & Marchitto, T. M. (2008). Mg/Ca-temperature proxy in benthic foraminifera: New calibrations from the Florida Straits and a hypothesis regarding Mg/Li. *Paleoceanography*, *23*, 1–17. https://doi.org/10.1029/2007PA001553

Coggon, R. M., Teagle, D., Smith-Duque, C., Alt, J., & Cooper, M. (2010). Reconstructing past seawater Mg/Ca. *Science*, *327*(5969), 1114–1117. https://doi.org/10.1126/science.1182252

Cramer, B. S., Toggweiler, J. R., Wright, J. D., Katz, M. E., & Miller, K. G. (2009). Ocean overturning since the late cretaceous: Inferences from a new benthic foraminiferal isotope compilation. *Paleoceanography*, *24*, 1–14. https://doi.org/10.1029/2008PA001683

Daëron, M., Blamart, D., Peral, M., & Affek, H. P. (2016). Absolute isotopic abundance ratios and the accuracy of Δ_{47} measurements. *Chemical Geology*, *442*, 83–96. https://doi.org/10.1016/j.chemgeo.2016.08.014

De Carlo, E. H. (1992). Geochemistry of pore water and sediments recovered from the Exmouth Plateau. In B. U. Haq, U. Von Rad, S. O'Connell, A. Bent, C. D. Blome, P. E. Borella, et al. (Eds.), *Proceedings of the Ocean Drilling Program, Scientific Results* (Vol. 122, pp. 295–308). College Station, TX: Ocean Drilling Program.

Defliese, W. F., & Lohmann, K. C. (2015). Non-linear mixing effects on mass-47 CO_2 clumped isotope thermometry: Patterns and implications. *Rapid Communications in Mass Spectrometry*, *29*(9), 901–909. https://doi.org/10.1002/rcm.7175

Dennis, K. J., Affek, H. P., Passey, B. H., Schrag, D. P., & Eiler, J. M. (2011). Defining an absolute reference frame for "clumped" isotope studies of CO_2. *Geochimica et Cosmochimica Acta*, *75*(22), 7117–7131. https://doi.org/10.1016/j.gca.2011.09.025

Denton, G. H., Prentice, M. L., Kellogg, D. E., & Kellogg, T. B. (1984). Late Tertiary history of the Antarctic ice sheet: Evidence from the Dry Valleys. *Geology*, *12*(5), 263–267. https://doi.org/10.1130/0091-7613(1984)12<263:LTHOTA>2.0.CO;2

Denton, G. H., & Sugden, D. E. (2005). Meltwater features that suggest Miocene ice-sheet overriding of the Transantarctic Mountains in Victoria Land, Antarctica. *Geografiska Annaler: Series A*, *87*(1), 67–85. 10.1111/j.0435-3676.2005.00245.x

Eagle, R. A., Eiler, J. M., Tripati, A. K., Ries, J. B., Freitas, P. S., Hiebenthal, C., et al. (2013). The influence of temperature and seawater carbonate saturation state on ^{13}C–^{18}O bond ordering in bivalve mollusks. *Biogeosciences*, *10*(7), 4591–4606. https://doi.org/10.5194/bg-10-4591-2013

Edgar, K. M., Pälike, H., & Wilson, P. A. (2013). Testing the impact of diagenesis on the $\delta^{18}O$ and $\delta^{13}C$ of benthic foraminiferal calcite from a sediment burial depth transect in the equatorial Pacific. *Paleoceanography*, *28*(3), 468–480. https://doi.org/10.1002/palo.20045

Eiler, J. M. (2007). "Clumped-isotope" geochemistry—The study of naturally-occurring, multiply-substituted isotopologues. *Earth and Planetary Science Letters*, *262*(3–4), 309–327. https://doi.org/10.1016/j.epsl.2007.08.020

Eiler, J. M. (2011). Paleoclimate reconstruction using carbonate clumped isotope thermometry. *Quaternary Science Reviews*, *30*(25–26), 3575–3588. https://doi.org/10.1016/j.quascirev.2011.09.001

Elderfield, H., Yu, J., Anand, P., Kiefer, T., & Nyland, B. (2006). Calibrations for benthic foraminiferal Mg/Ca paleothermometry and the carbonate ion hypothesis. *Earth and Planetary Science Letters*, *250*(3–4), 633–649. https://doi.org/10.1016/j.epsl.2006.07.041

Evans, D., Badger, M. P. S., Foster, G. L., Henehan, M. J., Lear, C. H., & Zachos, J. C. (2018). No substantial long-term bias in the Cenozoic benthic foraminifera oxygen-isotope record. *Nature Communications*, *9*(1), 2874. https://doi.org/10.1038/s41467-018-05304-3

Evans, D., & Müller, W. (2012). Deep time foraminifera Mg/Ca paleothermometry: Nonlinear correction for secular change in seawater Mg/Ca. *Paleoceanography*, *27*(4), 1–11. https://doi.org/10.1029/2012PA002315

Evans, D., Müller, W., & Erez, J. (2018). Assessing foraminifera biomineralisation models through trace element data of cultures under variable seawater chemistry. *Geochimica et Cosmochimica Acta*, *236*, 198–217. https://doi.org/10.1016/j.gca.2018.02.048

Evans, D., Sagoo, N., Renema, W., Cotton, L. J., Müller, W., Todd, J. A., et al. (2018). Eocene greenhouse climate revealed by coupled clumped isotope-Mg/Ca thermometry. *Proceedings of the National Academy of Sciences*, *115*(6), 1174–1179. https://doi.org/10.1073/pnas.1714744115

Evans, D., Wade, B. S., Henehan, M., Erez, J., & Müller, W. (2016). Revisiting carbonate chemistry controls on planktic foraminifera Mg/Ca: Implications for sea surface temperature and hydrology shifts over the Paleocene-Eocene Thermal Maximum and Eocene-Oligocene transition. *Climate of the Past*, *12*(4), 819–835. https://doi.org/10.5194/cp-12-819-2016

Exon, N. F., Haq, B. U., & Von Rad, U. (1992). Exmouth Plateau revisited: Scientific drilling and geological framework. In B. U. Haq, U. Von Rad, S. O'Connell, A. Bent, C. D. Blome, P. E. Borella, et al. (Eds.), *Proceedings of the Ocean Drilling Program, Scientific Results* (Vol. 122, pp. 3–20). College Station, TX: Ocean Drilling Program.

Feakins, S. J., Warny, S., & Lee, J. E. (2012). Hydrologic cycling over Antarctica during the middle Miocene warming. *Nature Geoscience*, *5*(8), 557–560. https://doi.org/10.1038/ngeo1498

Fernandez, A., Müller, I. A., Rodríguez-Sanz, L., van Dijk, J., Looser, N., & Bernasconi, S. M. (2017). A reassessment of the precision of carbonate clumped isotope measurements: Implications for calibrations and paleoclimate reconstructions. *Geochemistry, Geophysics, Geosystems*, *18*, 4375–4386. https://doi.org/10.1002/2017GC007106

Fielding, C. R., Browne, G. H., Field, B., Florindo, F., Harwood, D. M., Krissek, L. A., et al. (2011). Sequence stratigraphy of the ANDRILL AND-2A drillcore, Antarctica: A long-term, ice-proximal record of Early to Mid-Miocene climate, sea-level and glacial dynamism. *Palaeogeography, Palaeoclimatology, Palaeoecology*, *305*(1–4), 337–351. https://doi.org/10.1016/j.palaeo.2011.03.026

Flower, B. P., & Kennett, J. P. (1995). Middle Miocene deepwater paleoceanography in the southwest Pacific: Relations with East Antarctic Ice Sheet development. *Paleoceanography*, *10*(6), 1095–1112. https://doi.org/10.1029/95PA02022

Gasson, E., DeConto, R. M., Pollard, D., & Levy, R. H. (2016). Dynamic Antarctic ice sheet during the early to mid-Miocene. *Proceedings of the National Academy of Sciences*, *113*(13), 3459–3464. https://doi.org/10.1073/pnas.1516130113

Grauel, A. L., Schmid, T. W., Hu, B., Bergami, C., Capotondi, L., Zhou, L., & Bernasconi, S. M. (2013). Calibration and application of the "clumped isotope" thermometer to foraminifera for high-resolution climate reconstructions. *Geochimica et Cosmochimica Acta*, *108*, 125–140. https://doi.org/10.1016/j.gca.2012.12.049

Gray, W. R., Weldeab, S., Lea, D. W., Rosenthal, Y., Gruber, N., Donner, B., & Fischer, G. (2018). The effects of temperature, salinity, and the carbonate system on Mg/Ca in *Globigerinoides ruber* (white): A global sediment trap calibration. *Earth and Planetary Science Letters*, *482*, 607–620. https://doi.org/10.1016/j.epsl.2017.11.026

Greenop, R., Foster, G. L., Wilson, P. A., & Lear, C. H. (2014). Middle Miocene climate instability associated with high-amplitude CO_2 variability. *Paleoceanography*, *29*(9), 845–853. https://doi.org/10.1002/2014PA002653

Hall, J. M., & Chan, L. H. (2004). Li/Ca in multiple species of benthic and planktonic foraminifera: Thermocline, latitudinal, and glacial-interglacial variation. *Geochimica et Cosmochimica Acta*, *68*(3), 529–545. https://doi.org/10.1016/S0016-7037(00)00451-4

Leutert, T. J., Auderset, A., Martínez-García, A., Modestou, S., & Meckler, A. N. (2020). Coupled Southern Ocean cooling and Antarctic ice sheet expansion during the middle Miocene. *Nature Geoscience*, *13*(9), 634–639. https://doi.org/10.1038/s41561-020-0623-0

Hauptvogel, D. W., & Passchier, S. (2012). Early-Middle Miocene (17–14 Ma) Antarctic ice dynamics reconstructed from the heavy mineral provenance in the AND-2A drill core, Ross Sea, Antarctica. *Global and Planetary Change*, *82–83*, 38–50. https://doi.org/10.1016/j.gloplacha.2011.11.003

He, B., Olack, G. A., & Colman, A. S. (2012). Pressure baseline correction and high-precision CO_2 clumped-isotope (δ_{47}) measurements in bellows and micro-volume modes. *Rapid Communications in Mass Spectrometry*, *26*(24), 2837–2853. https://doi.org/10.1002/rcm.6436

Hilgen, F. J., Lourens, L. J., Van Dam, J. A., Beu, A. G., Boyes, A. F., Cooper, R. A., et al. (2012). The Neogene period. In F. M. Gradstein, J. G. Ogg, M. D. Schmitz, & G. M. Ogg (Eds.), *The Geologic Time Scale 2012* (Vol. 1–2, pp. 923–978). Amsterdam: Elsevier.

Hill, P. S., Tripati, A. K., & Schauble, E. A. (2014). Theoretical constraints on the effects of pH, salinity, and temperature on clumped isotope signatures of dissolved inorganic carbon species and precipitating carbonate minerals. *Geochimica et Cosmochimica Acta*, *125*, 610–652. https://doi.org/10.1016/j.gca.2013.06.018

Holbourn, A., Kuhnt, W., Frank, M., & Haley, B. A. (2013). Changes in Pacific Ocean circulation following the Miocene onset of permanent Antarctic ice cover. *Earth and Planetary Science Letters*, *365*, 38–50. https://doi.org/10.1016/j.epsl.2013.01.020

Holbourn, A., Kuhnt, W., Simo, J. A., & Li, Q. (2004). Middle Miocene isotope stratigraphy and paleoceanographic evolution of the northwest and southwest Australian margins (Wombat Plateau and Great Australian Bight). *Palaeogeography, Palaeoclimatology, Palaeoecology*, *208*(1–2), 1–22. https://doi.org/10.1016/j.palaeo.2004.02.003

Hollis, C. J., Dunkley Jones, T., Anagnostou, E., Bijl, P. K., Cramwinckel, M. J., Cui, Y., et al. (2019). The DeepMIP contribution to PMIP4: Methodologies for selection, compilation and analysis of latest Paleocene and early Eocene climate proxy data, incorporating version 0.1 of the DeepMIP database. *Geoscientific Model Development Discussion*, 1–98. https://doi.org/10.5194/gmd-2018-309

Horita, J., Zimmermann, H., & Holland, H. D. (2002). Chemical evolution of seawater during the Phanerozoic. *Geochimica et Cosmochimica Acta*, *66*(21), 3733–3756. https://doi.org/10.1016/s0016-7037(01)00884-5

Hu, B., Radke, J., Schlüter, H. J., Heine, F. T., Zhou, L., & Bernasconi, S. M. (2014). A modified procedure for gas-source isotope ratio mass spectrometry: The long-integration dual-inlet (LIDI) methodology and implications for clumped isotope measurements. *Rapid Communications in Mass Spectrometry*, *28*(13), 1413–1425. https://doi.org/10.1002/rcm.6909

Huntington, K. W., Eiler, J. M., Affek, H. P., Guo, W., Bonifacie, M., Yeung, L. Y., et al. (2009). Methods and limitations of "clumped" CO_2 isotope (Δ_{47}) analysis by gas-source isotope ratio mass spectrometry. *Journal of Mass Spectrometry*, *44*(9), 1318–1329. https://doi.org/10.1002/jms.1614

Ji, S., Nie, J., Lechler, A., Huntington, K. W., Heitmann, E. O., & Breecker, D. O. (2018). A symmetrical CO_2 peak and asymmetrical climate change during the middle Miocene. *Earth and Planetary Science Letters*, *499*, 134–144. https://doi.org/10.1016/j.epsl.2018.07.011

John, C. M., & Bowen, D. (2016). Community software for challenging isotope analysis: First applications of 'Easotope' to clumped isotopes. *Rapid Communications in Mass Spectrometry*, *30*(21), 2285–2300. https://doi.org/10.1002/rcm.7720

Kasbohm, J., & Schoene, B. (2018). Rapid eruption of the Columbia River flood basalt and correlation with the mid-Miocene climate optimum. *Science Advances*, *4*(9), eaat8223. https://doi.org/10.1126/sciadv.aat8223

Kele, S., Breitenbach, S. F. M., Capezzuoli, E., Nele Meckler, A., Ziegler, M., Millan, I. M., et al. (2015). Temperature dependence of oxygen- and clumped isotope fractionation in carbonates: A study of travertines and tufas in the 6–95°C temperature range. *Geochimica et Cosmochimica Acta*, *168*, 172–192. https://doi.org/10.1016/j.gca.2015.06.032

Kelson, J. R., Huntington, K. W., Schauer, A. J., Saenger, C., & Lechler, A. R. (2017). Toward a universal carbonate clumped isotope calibration: Diverse synthesis and preparatory methods suggest a single temperature relationship. *Geochimica et Cosmochimica Acta*, *197*, 104–131. https://doi.org/10.1016/j.gca.2016.10.010

Kender, S., Yu, J., & Peck, V. L. (2014). Deep ocean carbonate ion increase during mid Miocene CO_2 decline. *Scientific Reports*, *4*(Ccd), 1–6. https://doi.org/10.1038/srep04187

Kochhann, K. G. D., Holbourn, A., Kuhnt, W., Channell, J. E. T., Lyle, M., Shackford, J. K., et al. (2016). Eccentricity pacing of eastern equatorial Pacific carbonate dissolution cycles during the Miocene Climatic Optimum. *Paleoceanography*, *31*(9), 1176–1192. https://doi.org/10.1002/2016PA002988.Received

Kocken, I. J., Müller, I. A., & Zeigler, M. (2019). Optimizing the use of carbonate standards to minimize uncertainties in clumped isotope data. *Geochemistry, Geophysics, Geosystems*, *20*, 5565–5577. https://doi.org/10.1029/2019GC008545

Kozdon, R., Kelly, D. C., Kitajima, K., Strickland, A., Fournelle, J. H., & Valley, J. W. (2013). In situ $\delta^{18}O$ and Mg/Ca analyses of diagenetic and planktic foraminiferal calcite preserved in a deep-sea record of the Paleocene-Eocene thermal maximum. *Paleoceanography*, *28*(3), 517–528. https://doi.org/10.1002/palo.20048

Kürschner, W. M., Kvaček, Z., & Dilcher, D. L. (2008). The impact of Miocene atmospheric carbon dioxide fluctuations on climate and the evolution of terrestrial ecosystems. *Proceedings of the National Academy of Sciences of the United States of America*, *105*(2), 449–453. https://doi.org/10.1073/pnas.0708588105

Lammers, L. N., & Mitnick, E. H. (2019). Magnesian calcite solid solution thermodynamics inferred from authigenic deep-sea carbonate. *Geochimica et Cosmochimica Acta*, *248*, 343–355. https://doi.org/10.1016/j.gca.2019.01.006

Langebroek, P. M., Paul, A., & Schulz, M. (2009). Antarctic ice-sheet response to atmospheric CO_2 and insolation in the middle Miocene. *Climate of the Past*, *5*(4), 633–646. https://doi.org/10.5194/cp-5-633-2009

Larsen, H. C., Saunders, A. D., Clift, P. D., Beget, J., Wei, W., & Spezzaferri, S. S. (1994). Seven million years of glaciation in Greenland. *Science*, *264*(5161), 952–955. https://doi.org/10.1126/science.264.5161.952

Lear, C. H., Coxall, H. K., Foster, G. L., Lunt, D. J., Mawbey, E. M., Rosenthal, Y., et al. (2015). Neogene ice volume and ocean temperatures: Insights from infaunal foraminiferal Mg/Ca paleothermometry. *Paleoceanography*, *30*(11), 1437–1454. https://doi.org/10.1002/2015PA002833

Lear, C. H., Elderfield, H., & Wilson, P. A. (2000). Cenozoic deep-sea temperatures and global ice volumes from Mg/Ca in benthic foraminiferal calcite. *Science*, *287*(5451), 269–272. https://doi.org/10.1126/science.287.5451.269

Lear, C. H., Mawbey, E. M., & Rosenthal, Y. (2010). Cenozoic benthic foraminiferal Mg/Ca and Li/Ca records: Toward unlocking temperatures and saturation states. *Paleoceanography*, *25*, 1–11. https://doi.org/10.1029/2009PA001880

Lear, C. H., & Rosenthal, Y. (2006). Benthic foraminiferal Li/Ca: Insights into Cenozoic seawater carbonate saturation state. *Geology*, *34*(11), 985–988. https://doi.org/10.1130/G22792A.1

Lear, C. H., Rosenthal, Y., & Slowey, N. (2002). Benthic foraminiferal Mg/Ca-paleothermometry: A revised core-top calibration. *Geochimica et Cosmochimica Acta*, *66*(19), 3375–3387. https://doi.org/10.1016/S0016-7037(02)00941-9

Leutert, T. J., Sexton, P. F., Tripati, A. K., Piasecki, A., Ho, S. L., & Meckler, A. N. (2019). Sensitivity of clumped isotope temperatures in fossil benthic and planktic foraminifera to diagenetic alteration. *Geochimica et Cosmochimica Acta*, *257*, 354–372. https://doi.org/10.1016/j.gca.2019.05.005

Levy, R., Harwood, D., Florindo, F., Sangiorgi, F., Tripati, R., von Eynatten, H., et al. (2016). Antarctic ice sheet sensitivity to atmospheric CO_2 variations in the early to mid-Miocene. *Proceedings of the National Academy of Sciences*, *113*(13), 3453–3458. https://doi.org/10.1073/pnas.1516030113

Lewis, A. R., Marchant, D. R., Ashworth, A. C., Hedenäs, L., Hemming, S. R., Johnson, J. V., et al. (2008). Mid-Miocene cooling and the extinction of tundra in continental Antarctica. *Proceedings of the National Academy of Sciences*, *105*(31), 10,676–10,680. https://doi.org/10.1073/pnas.0802501105

Lowenstein, T. K., Timofeeff, M. N., Brennan, S. T., Hardie, L. A., & Demicco, R. V. (2001). Oscillations in Phanerozoic seawater chemistry: Evidence from fluid inclusions. *Science*, *294*(5544), 1086–1088. https://doi.org/10.1126/science.1064280

Marchitto, T. M., Bryan, S. P., Curry, W. B., & McCorkle, D. C. (2007). Mg/Ca temperature calibration for the benthic foraminifer *Cibicidoides pachyderma*. Paleoceanography, *22*, 1–9. https://doi.org/10.1029/2006PA001287

Marchitto, T. M., Curry, W. B., Lynch-Stieglitz, J., Bryan, S. P., Cobb, K. M., & Lund, D. C. (2014). Improved oxygen isotope temperature calibrations for cosmopolitan benthic foraminifera. *Geochimica et Cosmochimica Acta*, *130*, 1–11. https://doi.org/10.1016/j.gca.2013.12.034

Marriott, C. S., Henderson, G. M., Crompton, R., Staubwasser, M., & Shaw, S. (2004). Effect of mineralogy, salinity, and temperature on Li/Ca and Li isotope composition of calcium carbonate. *Chemical Geology*, *212*(1–2), 5–15. https://doi.org/10.1016/j.chemgeo.2004.08.002

Matthews, K. J., Maloney, K. T., Zahirovic, S., Williams, S. E., Seton, M., & Müller, R. D. (2016). Global plate boundary evolution and kinematics since the late Paleozoic. *Global and Planetary Change*, *146*, 226–250. https://doi.org/10.1016/j.gloplacha.2016.10.002

Meckler, A. N., Ziegler, M., Millán, M. I., Breitenbach, S. F. M., & Bernasconi, S. M. (2014). Long-term performance of the Kiel carbonate device with a new correction scheme for clumped isotope measurements. *Rapid Communications in Mass Spectrometry*, *28*(15), 1705–1715. https://doi.org/10.1002/rcm.6949

Meinicke, N., Ho, S. L., Hannisdal, B., Nürnberg, D., Tripati, A. K., Schiebel, R., & Meckler, A. N. (2020). A robust calibration of the clumped isotopes to temperature relationship for foraminifers. *Geochimica et Cosmochimica Acta*, *270*, 160–183. https://doi.org/10.1016/j.gca.2019.11.022

Mudelsee, M., Bickert, T., Lear, C. H., & Lohmann, G. (2014). Reviews of geophysics Cenozoic climate changes: A review based on time series analysis of marine benthic δ^{18}O records. *Reviews of Geophysics*, *52*, 333–374. https://doi.org/10.1002/2013RG000440. Received

Müller, I. A., Fernandez, A., Radke, J., van Dijk, J., Bowen, D., Schwieters, J., & Bernasconi, S. M. (2017). Carbonate clumped isotope analyses with the long-integration dual-inlet (LIDI) workflow: Scratching at the lower sample weight boundaries. *Rapid Communications in Mass Spectrometry*, *31*(12), 1057–1066. https://doi.org/10.1002/rcm.7878

Nairn, M. G., Lear, C. H., Sosdian, S. M., Bailey, T. R., & Beavington-Penney, S. (2020). Tropical sea surface temperatures following the middle Miocene climate transition from laser-ablation ICP-MS analysis of diagenetically coated foraminifera. *Paleoceanography and Paleoclimatology*. https://doi.org/10.1002/essoar.10502707.1

Party, S. S. (1990). Site 761. In B. U. Haq, U. Von Rad, S. O'Connell, A. Bent, C. D. Blome, P. E. Borella, et al. (Eds.), *Proceedings of Ocean Drilling Program Leg 122, Initial Results* (pp. 161–211). College Station, TX (Ocean Drilling Program): Ocean Drilling Program.

Passchier, S., Browne, G., Field, B., Fielding, C. R., Krissek, L. A., Panter, K., & Pekar, S. F. (2011). Early and middle Miocene Antarctic glacial history from the sedimentary facies distribution in the AND-2A drill hole, Ross Sea, Antarctica. *Bulletin of the Geological Society of America*, *123*(11–12), 2352–2365. https://doi.org/10.1130/B30334.1

Peral, M., Daëron, M., Blamart, D., Bassinot, F., Dewilde, F., Smialkowski, N., et al. (2018). Updated calibration of the clumped isotope thermometer in planktonic and benthic foraminifera. *Geochimica et Cosmochimica Acta*, *239*, 1–16. https://doi.org/10.1016/j.gca.2018.07.016

Piasecki, A., Bernasconi, S. M., Grauel, A., Hannisdal, B., Ho, S. L., Leutert, T. J., et al. (2019). Application of clumped isotope thermometry to benthic foraminifera. *Geochemistry, Geophysics, Geosystems*, *20*, 2082–2090. https://doi.org/10.1029/2018GC007961

Pierce, E. L., van de Flierdt, T., Williams, T., Hemming, S. R., Cook, C. P., & Passchier, S. (2017). Evidence for a dynamic East Antarctic ice sheet during the mid-Miocene climate transition. *Earth and Planetary Science Letters*, *478*, 1–13. https://doi.org/10.1016/j.epsl.2017.08.011

Pound, M. J., Haywood, A. M., Salzmann, U., & Riding, J. B. (2012). Global vegetation dynamics and latitudinal temperature gradients during the Mid to Late Miocene (15.97–5.33Ma). *Earth-Science Reviews*, *112*(1–2), 1–22. https://doi.org/10.1016/j.earscirev.2012.02.005

Ramsay, T. S., Smart, C. W., & Zachos, J. C. (1998). A model of early to middle Miocene Deep Ocean circulation for the Atlantic and Indian oceans. *Geological Society of London, Special Publication*, *131*(1), 55–70. https://doi.org/10.1144/GSL.SP.1998.131.01.04

Rodríguez-Sanz, L., Bernasconi, S. M., Marino, G., Heslop, D., Müller, I. A., Fernandez, A., et al. (2017). Penultimate deglacial warming across the Mediterranean Sea revealed by clumped isotopes in foraminifera. *Scientific Reports*, *7*(1), 16,572–16,511. https://doi.org/10.1038/s41598-017-16528-6

Saenger, C., Affek, H. P., Felis, T., Thiagarajan, N., Lough, J. M., & Holcomb, M. (2012). Carbonate clumped isotope variability in shallow water corals: Temperature dependence and growth-related vital effects. *Geochimica et Cosmochimica Acta*, *99*, 224–242. https://doi.org/10.1016/j.gca.2012.09.035

Sames, B., Wagreich, M., Conrad, C. P., & Iqbal, S. (2020). Aquifer-eustasy as the main driver of short-term sea-level fluctuations during Cretaceous hothouse climate phases. *Geological Society, London, Special Publications*, *498*(1), 9–38. https://doi.org/10.1144/SP498-2019-105

Sangiorgi, F., Bijl, P. K., Passchier, S., Salzmann, U., Schouten, S., McKay, R., et al. (2018). Southern Ocean warming and Wilkes Land ice sheet retreat during the mid-Miocene. *Nature Communications*, *9*(1), 317–311. https://doi.org/10.1038/s41467-017-02609-7

Schlitzer, R. (2020). *Ocean Data View*. Retrieved from https://odv.awi.de

Schauble, E. A., Ghosh, P., & Eiler, J. M. (2006). Preferential formation of ^{13}C–^{18}O bonds in carbonate minerals, estimated using first-principles lattice dynamics. *Geochimica et Cosmochimica Acta*, *70*(10), 2510–2529. https://doi.org/10.1016/j.gca.2006.02.011

Sexton, P. F., Wilson, P. A., & Pearson, P. N. (2006). Microstructural and geochemical perspectives on planktic foraminiferal preservation: "Glassy" versus "frosty". *Geochemistry, Geophysics, Geosystems*, *7*, Q12P19. https://doi.org/10.1029/2006GC001291

Shackleton, N. J., Hall, M. A., & Boersma, A. (1984). 15. Oxygen and carbon isotope data from Leg 74 foraminifers. In T. C. Moore, P. D. Rabinowitz, P. Borelly, A. Boersma, & N. J. Shackleton (Eds.), *Initial Reports of the Deep Sea Drilling Project* (Vol. 74, pp. 599–612). Washington: U.S. Government Printing Office. https://doi.org/10.2973/dsdp.proc.74.115.1984

Shevenell, A. E., & Kennett, J. P. (2004). Paleoceanographic change during the middle Miocene climate revolution: An Antarctic stable isotope perspective. In N. F. Exon, J. P. Kennett, & M. J. Malone (Eds.), *The Cenozoic Southern Ocean: Tectonics, sedimentation, and climate change between Australia and Antarctica*, *Geophysical Monograph Series* (Vol. 151, pp. 235–251). Washington, DC: American Geophysical Union. https://doi.org/10.1029/151GM14

Shevenell, A. E., & Kennett, J. P. (2007). Cenozoic Antarctic cryosphere evolution: Tales from deep-sea sedimentary records. *Deep-Sea Research Part II: Topical Studies in Oceanography*, *54*(21–22), 2308–2324. https://doi.org/10.1016/j.dsr2.2007.07.018

Shevenell, A. E., Kennett, J. P., & Lea, D. W. (2008). Middle Miocene ice sheet dynamics, deep-sea temperatures, and carbon cycling: A Southern Ocean perspective. *Geochemistry, Geophysics, Geosystems*, 9, Q02006. https://doi.org/10.1029/2007GC001736

Sosdian, S. M., Greenop, R., Hain, M. P., Foster, G. L., Pearson, P. N., & Lear, C. H. (2018). Constraining the evolution of Neogene ocean carbonate chemistry using the boron isotope pH proxy. *Earth and Planetary Science Letters*, 498, 362–376. https://doi.org/10.1016/J.EPSL.2018.06.017

Spero, H. J., Bijma, J., Lea, D. W., & Bemis, B. E. (1997). Effect of seawater carbonate concentration on foraminiferal carbon and oxygen isotopes. *Nature*, 390(6659), 497–500. https://doi.org/10.1038/37333

Stolper, D. A., Eiler, J. M., & Higgins, J. A. (2018). Modeling the effects of diagenesis on carbonate clumped-isotope values in deep- and shallow-water settings. *Geochimica et Cosmochimica Acta*, 227, 264–291. https://doi.org/10.1016/j.gca.2018.01.037

Super, J. R., Thomas, E., Pagani, M., Huber, M., Brien, C. O., & Hull, P. M. (2018). North Atlantic temperature and pCO_2 coupling in the early-middle Miocene. *Geology*, 46(6), 519–522. https://doi.org/10.1130/G40228.1

Tang, J., Dietzel, M., Fernandez, A., Tripati, A. K., & Rosenheim, B. E. (2014). Evaluation of kinetic effects on clumped isotope fractionation (δ_{47}) during inorganic calcite precipitation. *Geochimica et Cosmochimica Acta*, 134, 120–136. https://doi.org/10.1016/j.gca.2014.03.005

Tierney, J. E., Malevich, S. B., Gray, W., Vetter, L., & Thirumalai, K. (2019). Bayesian calibration of the Mg/Ca Paleothermometer in Planktic Foraminifera. *Paleoceanography and Paleoclimatology*, 34(12), 2005–2030. https://doi.org/10.1029/2019PA003744

Tripati, A. K., Eagle, R. A., Thiagarajan, N., Gagnon, A. C., Bauch, H., Halloran, P. R., & Eiler, J. M. (2010). $^{13}C–^{18}O$ isotope signatures and "clumped isotope" thermometry in foraminifera and coccoliths. *Geochimica et Cosmochimica Acta*, 74(20), 5697–5717. https://doi.org/10.1016/j.gca.2010.07.006

Tripati, A. K., Hill, P. S., Eagle, R. A., Mosenfelder, J. L., Tang, J., Schauble, E. A., et al. (2015). Beyond temperature: Clumped isotope signatures in dissolved inorganic carbon species and the influence of solution chemistry on carbonate mineral composition. *Geochimica et Cosmochimica Acta*, 166, 344–371. https://doi.org/10.1016/j.gca.2015.06.021

Tripati, A. K., Sahany, S., Pittman, D., Eagle, R. A., Neelin, J. D., Mitchell, J. L., & Beaufort, L. (2014). Modern and glacial tropical snowlines controlled by sea surface temperature and atmospheric mixing. *Nature Geoscience*, 7(3), 205–209. https://doi.org/10.1038/ngeo2082

Uchikawa, J., & Zeebe, R. E. (2010). Examining possible effects of seawater pH decline on foraminiferal stable isotopes during the Paleocene-Eocene Thermal Maximum. *Paleoceanography*, 25, 1–14. https://doi.org/10.1029/2009PA001864

Van Hinsbergen, D. J. J., De Groot, L. V., Van Schaik, S. J., Spakman, W., Bijl, P. K., Sluijs, A., et al. (2015). A paleolatitude calculator for paleoclimate studies. *PLoS ONE*, 10(6), e0126946. https://doi.org/10.1371/journal.pone.0126946

Voigt, J., Hathorne, E. C., Frank, M., & Holbourn, A. (2016). Minimal influence of recrystallization on middle Miocene benthic foraminiferal stable isotope stratigraphy in the eastern equatorial Pacific. *Paleoceanography*, 31(1), 98–114. https://doi.org/10.1002/2015PA002822

Voigt, J., Hathorne, E. C., Frank, M., Vollstaedt, H., & Eisenhauer, A. (2015). Variability of carbonate diagenesis in equatorial Pacific sediments deduced from radiogenic and stable Sr isotopes. *Geochimica et Cosmochimica Acta*, 148, 360–377. https://doi.org/10.1016/j.gca.2014.10.001

von Rad, U., Exon, N. F., & Haq, B. U. (1992). Rift-to-drift history of the Wombat Plateau, northwest Australia: Triassic to Tertiary Leg 122 results. In B. U. Haq, U. Von Rad, S. O'Connell, A. Bent, C. D. Blome, & P. E. Borella (Eds.), *Proceedings of the Ocean Drilling Program, Scientific Results* (Vol. 122, pp. 765–800). College Station, TX: Ocean Drilling Program. https://doi.org/10.2973/odp.proc.sr.122.181.1992

Warny, S., Askin, R. A., Hannah, M. J., Mohr, B. A. R., Raine, J. I., Harwood, D. M., & Florindo, F. (2009). Palynomorphs from a sediment core reveal a sudden remarkably warm Antarctica during the middle Miocene. *Geology*, 37(10), 955–958. https://doi.org/10.1130/G30139A.1

Watkins, J. M., & Hunt, J. D. (2015). A process-based model for non-equilibrium clumped isotope effects in carbonates. *Earth and Planetary Science Letters*, 432, 152–165. https://doi.org/10.1016/j.epsl.2015.09.042

Woodruff, F., & Savin, S. M. (1989). Miocene deepwater oceanography. *Paleoceanography*, 4(1), 87–140. https://doi.org/10.1029/PA004i001p00087

You, Y., Huber, M., Müller, R. D., Poulsen, J., & Ribbe, J. (2009). Simulation of the middle Miocene climate optimum. *Geophysical Research Letters*, 36, L04702. https://doi.org/10.1029/2008GL036571

Yu, J., & Elderfield, H. (2008). Mg/Ca in the benthic foraminifera *Cibicidoides wuellerstorfi* and *Cibicidoides mundulus*: Temperature versus carbonate ion saturation. *Earth and Planetary Science Letters*, 116(C12), 129–139. https://doi.org/10.1029/2011JC007255

Zachos, J. C., Dickens, G. R., & Zeebe, R. E. (2008). An early Cenozoic perspective on greenhouse warming and carbon-cycle dynamics. *Nature*, 451(7176), 279–283. https://doi.org/10.1038/nature06588

Zeebe, R. E. (1999). An explanation of the effect of seawater carbonate concentration on foraminiferal oxygen isotopes. *Geochimica et Cosmochimica Acta*, 63(13–14), 2001–2007. https://doi.org/10.1016/S0016-7037(99)00091-5

Zhang, Y. G., Pagani, M., Liu, Z., Bohaty, S. M., & Deconto, R. (2013). A 40-million-year history of atmospheric CO_2. *Philosophical Transactions of the Royal Society A: Mathematical, Physical and Engineering Sciences*, 371(2001), 20130096. https://doi.org/10.1098/rsta.2013.0096